AD_____

GRANT NO: DAMD17-94-J-4144
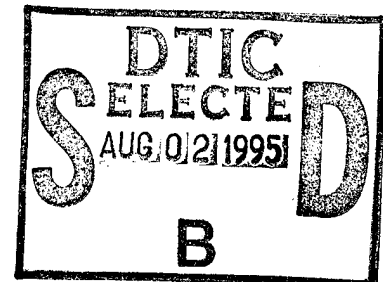
TITLE: An Examination of Ultrasound Measured Tissue Perfusion on Breast Cancer

PRINCIPAL INVESTIGATOR: Jeffrey Brian Fowlkes, Ph.D.
                           Paul L. Carson, Ph.D.

CONTRACTING ORGANIZATION: University of Michigan
                             Ann Arbor, MI 48109-0553

REPORT DATE: 7/1/95

TYPE OF REPORT: Annual

PREPARED FOR: U.S. Army Medical Research and Materiel
                 Command
                 Fort Detrick, Maryland 21702-5012

DISTRIBUTION STATEMENT: Approved for public release;
                           distribution unlimited

19950801 021

DTIC QUALITY INSPECTED 1

REPORT DOCUMENTATION PAGE

Public reporting burden for this collection of information is estimated to average 1 hour per response, including the time for reviewing instructions, searching existing data sources, gathering and maintaining the data needed, and completing and reviewing the collection of information. Send comments regarding this burden estimate or any other aspect of this collection of information, including suggestions for reducing this burden, to Washington Headquarters Services, Directorate for Information Operations and Reports, 1215 Jefferson Davis Highway, Suite 1204, Arlington, VA 22202-4302, and to the Office of Management and Budget, Paperwork Reduction Project (0704-0188), Washington, DC 20503.

1. AGENCY USE ONLY (Leave blank)	2. REPORT DATE 7/1/95	3. REPORT TYPE AND DATES COVERED Annual 1 Jun 94 – 31 May 95

4. TITLE AND SUBTITLE

An Examination of Ultrasound Measured Tissue Perfusion on Breast Cancer

5. FUNDING NUMBERS

DAMD17-94-J-4144

6. AUTHOR(S)

J. Brian Fowlkes, Ph.D.
Paul L. Carson, Ph.D.

7. PERFORMING ORGANIZATION NAME(S) AND ADDRESS(ES)

University of Michigan
Ann Arbor, MI 48109-0553

8. PERFORMING ORGANIZATION REPORT NUMBER

9. SPONSORING / MONITORING AGENCY NAME(S) AND ADDRESS(ES)

U.S. Army Medical Research and Materiel Command
Fort Detrick, Maryland 21702-5012

10. SPONSORING / MONITORING AGENCY REPORT NUMBER

11. SUPPLEMENTARY NOTES
NONE

12a. DISTRIBUTION / AVAILABILITY STATEMENT

Approved for public release; distribution unlimited

12b. DISTRIBUTION CODE

13. ABSTRACT (Maximum 200 words)

Mammography has proven to be reliable as a screening tool for breast cancer. However, the specificity of mammography for breast cancer may be as low as 10% as evidenced by the number of biopsies recommended compared to the number of cancers confirmed (Moskowitz and Gartside, 1982). The present research is design to aid diagnosis by developing techniques for ultrasonic measurement of tissue perfusion including ultrasound contrast agent interruption for more effective washin/washout studies, decorrelation techniques and combination of Doppler power and velocity information for perfusion-like measures.

Research thus far indicates that contrast interruption is possible *in vivo*, generating negative contrast boluses which are well resolved in time. Transcutaneous interruption of contrast further defines the circumstances relevant in a more complete study of the process *in vitro*. These studies should reduce the acoustic amplitude required to generate the bolus and to control the time course of the interruption.

The development of image-based slice positioning should provide a more accurate assessment of the tissue perfusion using the estimation techniques proposed in this research. Although this was not a specific goal of this research, the significance of this work may reach beyond the concepts originally proposed.

14. SUBJECT TERMS

Ultrasound, Perfusion, Blood Flow, Breast, Cancer

15. NUMBER OF PAGES
53

16. PRICE CODE

17. SECURITY CLASSIFICATION OF REPORT	18. SECURITY CLASSIFICATION OF THIS PAGE	19. SECURITY CLASSIFICATION OF ABSTRACT	20. LIMITATION OF ABSTRACT
Unclassified	Unclassified	Unclassified	Unlimited

FOREWORD

Opinions, interpretations, conclusions and recommendations are those of the author and are not necessarily endorsed by the US Army.

_____ Where copyrighted material is quoted, permission has been obtained to use such material.

_____ Where material from documents designated for limited distribution is quoted, permission has been obtained to use the material.

X Citations of commercial organizations and trade names in this report do not constitute an official Department of Army endorsement or approval of the products or services of these organizations.

X In conducting research using animals, the investigator(s) adhered to the "Guide for the Care and Use of Laboratory Animals," prepared by the Committee on Care and Use of Laboratory Animals of the Institute of Laboratory Resources, National Research Council (NIH Publication No. 86-23, Revised 1985).

X For the protection of human subjects, the investigator(s) adhered to policies of applicable Federal Law 45 CFR 46.

_____ In conducting research utilizing recombinant DNA technology, the investigator(s) adhered to current guidelines promulgated by the National Institutes of Health.

_____ In the conduct of research utilizing recombinant DNA, the investigator(s) adhered to the NIH Guidelines for Research Involving Recombinant DNA Molecules.

_____ In the conduct of research involving hazardous organisms, the investigator(s) adhered to the CDC-NIH Guide for Biosafety in Microbiological and Biomedical Laboratories.

PI - Signature   7/1/95   Date

TABLE OF CONTENTS

INTRODUCTION (excerpts from the original proposal)

Nature of the Problem

Mammography has proven to be reliable as a screening tool for breast cancer. However, the specificity of mammography for breast cancer may be as low as 10% as evidenced by the number of biopsies recommended compared to the number of cancers confirmed (Moskowitz and Gartside, 1982). Therefore, of significant health care benefit would be a method used in conjunction with mammography which could reduce the number of biopsies required while maintaining or improving survival rates. In terms of health care costs, Adler *et al.* (1990) estimated that more than half of the mammographic screening costs for breast cancer are the result of required biopsies or excisions due to low specificity. Again, an alternative method for establishing the type of lesion present would be of great benefit. Any improvement in early detection of breast cancer is clearly important as survival is significantly improved when cancers are detected in the 0.5 to 1 cm diameter size range (Axtel *et al*, 1976).

Background of Previous Work

Doppler ultrasound has been investigated and found some utility in the detection of cancer (Burns *et al*, 1982; Minasian and Bamber, 1982; Boyd *et al*, 1983) . Although the specificity has been high for cancer recognition, at 10 MHz frequencies used in these studies, the sensitivity of the technique has not and the use of other Doppler techniques have had mixed specificity and sensitivity results (Rubin *et al*, 1987; Adler *et al*, 1988; Jellins, 1988; Cosgrove *et al*, 1990; Adler *et al*, 1990). The advent of stable ultrasound contrast agents and the development of Doppler power mode imaging are clearly innovations which could improve the sensitivity of ultrasound techniques for cancer.

Abnormal accumulation of contrast during the arterial phase of contrast transit and a residual concentration of contrast agent in breast cancers has been observed with conventional angiography, but without exceptionally high specificity (Feldman *et al*, 1967; Kaushik *et al*, 1975; Sakki, 1974), with x-ray computed tomography (Chang *et al*, 1982) and with digital subtraction angiography (Flynn *et al.*, 1984). Gadolinium MRI is now looking quite positive as a means of discriminating likely breast cancers and even detecting mammographically occult malignancies (Harms, et al., 1993, Heywang-Kobrunner, et al., 1992). With the advent of ultrasound contrast, such contrast studies should now be possible. The desired IV administration of the agent however results in dilution of the contrast and the loss of a well resolved bolus. If such problems can be overcome, the prospect for ultrasound contrast detection of breast cancer would be greatly improved due to the increased signal strength from the smaller, more diagnostic vessels. Doppler power imaging has also demonstrated an improved signal to noise ratio over conventional color Doppler flow imaging. Images being made in this mode seem to indicate one can expect such a modality would improve on the sensitivity of ultrasound for small vessels.

Finally, recent work (Weidner *et al.*, 1991; Horak, 1992) concerning angiogenesis has placed renewed emphasis on the blood flow in the region of cancerous lesions. The potential of ultrasound techniques described in this proposal to measure regional perfusion suggests that information can be derived by noninvasive means using a relatively inexpensive imaging modality.

Purpose of Present Work

The present research is design to develop techniques for ultrasonic measurement of tissue perfusion in the breast. In combination with other information such as mammographic examination, the techniques proposed should have application in the detection of cancerous lesions or the monitoring of therapeutic interventions which affect the vascular flow of tumor tissue. The diagnostic specificity for cancer could be increased with these techniques leading to improved patient management while using an imaging modality which is generally less expensive than many alternatives.

Methods of Approach

This study examines the potential of three related Doppler techniques for measuring tissue perfusion. 1) Acoustic fields can be used to modulate a continuous infusion of bubble-based echocontrast agent to estimate wash in-wash out time courses for the agent. 2) The decorrelation time of the Doppler power signal can measure the regional perfusion based on the rate at which blood moves out of the Doppler sample volume. 3) The combination of Doppler signal power and velocity will be used to approximate the tissue perfusion where the Doppler signal power is normalized to that found in a large vessel near the region of interest. Development of these techniques will be through *ex vivo* and *in vivo* experimentation using simple and physiologically relevant flow phantom and animal studies. The latter two techniques described above will be examined in limited clinical trials within the time frame of this study.

DESCRIPTION OF RESEARCH PROGRESS

The following is a list of relevant publications which have resulted from this work.

Peer Reviewed Journal Articles
Adler RS, Rubin JM, Fowlkes JB, Carson PL, Pallister JE: Ultrasonic Estimation of Tissue Perfusion: A Stochastic Approach, Ultrasound Med. Biol. Vol. 21 (4), 493-500, 1995.

Rubin, JM, Adler RS, Fowlkes JB, Spratt S, Pallister JE, Chen JF, Carson PL: Fractional moving blood volume estimation using doppler power imaging, Radiology, accepted, 1995.

Abstracts and Proceedings
Fowlkes JB, Gardner EA, Carson PL, Ivey JA, Rubin JM: "Acoustic Interruption of Ultrasound Contrast Agents for Blood Flow Evaluation", Procs., 39th Annual Conv. of the American Institute of Ultrasound in Medicine, San Francisco, CA, March 26-29, 1995.

Rubin JM, Adler RS, Fowlkes JB, Spratt S, Pallister JE, Chen J-F, Carson PL (1995) Fractional Moving Blood Volume Estimation Using Doppler Power Imaging, Twentieth International Symposium on Ultrasonic Imaging and Tissue Characterization, Arlington, VA, Program and Abstracts, June 7-9, 1995.

Fowlkes JB, Gardner EA, Carson PL, Ivey A and Rubin JM: Use of Contrast Interruption in the Measurement of Blood Flow. Symposium on Ultrasonic Imaging and Tissue Characterization, Arlington, VA, June 7-9, 1995.

Fowlkes JB: Progress in Perfusion and Moving Fractional Blood Volume Estimation Using Doppler Imaging. Ninth International Congress on the Ultrasonic Examination of the Breast , Indianapolis, IN, Sept. 28-October 1, 1995.

Chen, JF, Fowlkes, JB, Carson, PL and Moskalik: Determination of Scanhead Motion Using Decorrelation of Speckle, AAPM 37th Annual Meeting and Exhibition, Boston, MA, July 23-27, 1994.

As is indicated above, this research project is divided into three components. Progress in each of these areas will now be discussed in turn. Two of the research areas have been combined in this writing. This method of relating the progress information is chosen for presentation purposes in this report given the considerable interaction between the different aspects of the project.

Contrast Manipulation

In the original proposal for the first year's effort, we had proposed a series of *ex vivo* measurements to examine the parameters which control contrast manipulation using acoustic fields. This was based on our previous observations made using flow in tubes. However, we were concerned that considerable effort could be spent examining the process under an initial set of conditions which might not be sufficiently like those found *in vivo*. We continue to see some differences in the case contrast agents interrupted in blood and in water during *ex vivo* experiments. Therefore, we conducted two initial *in vivo* experiments in conjunction with our other on going research in the area of ultrasound contrast agents. The following is a description of those experiments and the results of one of these is presented.

The first experiment was performed in a rabbit being a VX2 carcinoma in the right thigh. This animal was being used to evaluate an experimental ultrasound contrast agent, MRX-115 (ImaR$_x$ Pharmaceuticals, Tucson, AZ). The agent is a perfluorocarbon gas-filled microbubble which is stabilized with a lipid shell. It has a mean diameter of 2.5 μm and a bubble concentration of 1.5×10^9 bubbles/ml with 99% of those bubbles being < 10 μm in diameter. Figure 1 is a size distribution for the bubbles as measured using a Accusizer optical sizing system. For these experiments, a MRX-115 dose of 10 μl/kg was used for each injection into the ear vein through a catheter and followed by a saline flush. The animal was anesthetized using Ketamine (5 mg/kg) and Rompun (35 mg/kg) and the right leg shaved over the inner (over the femoral artery) and outer (over the VX2 carcinoma) thigh. Depilatory creme was applied to the skin surface to remove residual hair and the skin was washed with a surgical scrub and rinsed with a 1:200 dilute solution of PhotoFlo (Eastman Kodak, Rochester, NY), a surfactant to act as a wetting agent. The animal was then placed under the ultrasound system shown in Fig. 2 with the coupling bath over the inner thigh. This system was developed for transcutaneous bubble generation (Ivey *et al,* 1995) and uses a high powered coaxial transducer consisting of a piezoceramic, 67 mm-diameter outer element used for producing high amplitude fields and a 10 mm-diameter inner element of the same material used for pulse-echo alignment. The outer element operated at a center frequency of 1.8 MHz has a 25% bandwidth and a focal length of 6 cm. The transducer focal beam width and depth of focus were 1.1 mm and 7.8 mm, respectively at the -6 dB level. A single, sinusoidal tone burst was employed with durations up to 250 ms. The transducer was suspended vertically in a water standoff tank filled with degassed water, filtered at 0.2 μm. A 0.1 mm thick polyethylene sheet was used for the acoustically transparent bottom window of the water standoff.

The focal point of the power transducer was aligned at approximately the center of the femoral artery lumen using a Diasonics Spectra VST (Diasonics Ultrasound, Milipitas, CA) and its 7.5 MHz sector format endocavitary probe which was rigidly fixed to the transducer so that the axis of the power transducer was in the image plane. The image of a mechanical pointer placed on the power transducer face was used to mark the location in the image plane corresponding to the focus. The femoral artery was identified with the diagnostic scanner in Doppler mode and the combined transducer assembly was then positioned so that the femoral artery was at the point in the image marking the focal point of the power transducer.

An HP 3314 Function Generator (Hewlett Packard, Everette, WA) was trigger manually to produce the gating pulse to control the length of the RF burst output by the Wavetek Model 50 function generator (Wavetek Inc., San Diego, CA). The RF burst was amplified by an ENI A300 RF amplifier (ENI, Inc., Rochester, NY) and connected to the 1.8 MHz transducer through a matching circuit. A separate 10 MHz linear array on the Diasonics scanner, operating typically at 6 MHz for Doppler modes was placed over a distal artery in the VX2 carcinoma and used in the spectral Doppler mode.
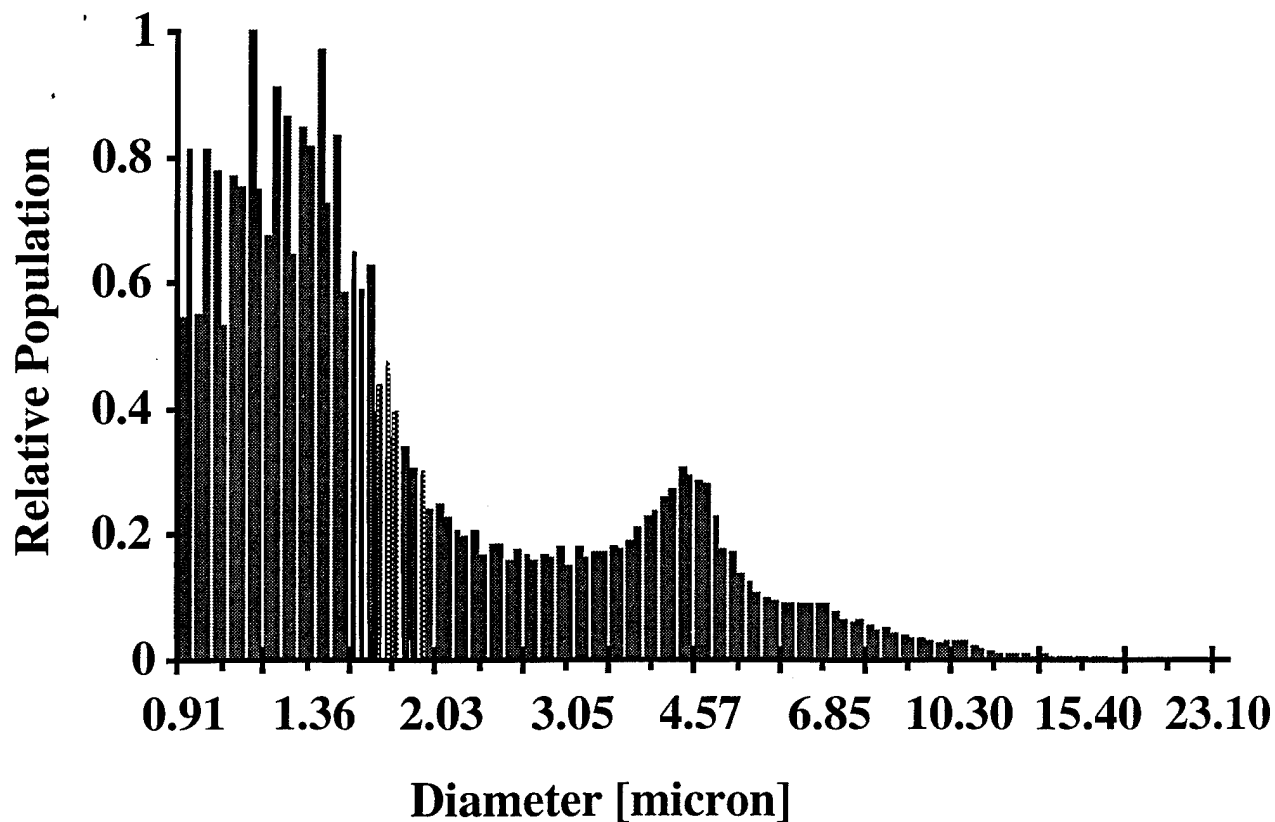
Figure 1 - Size distribution for the MRX-115 contrast agent used for *in vivo* contrast interruption.
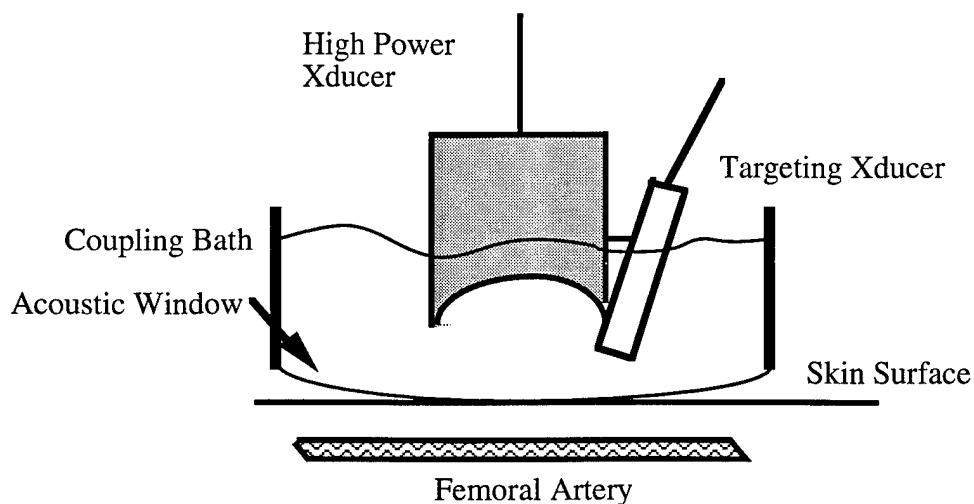

Figure 2 - Transcutaneous contrast interruption setup using high power transducer to halt the flow of contrast injected IV in the ear vein of a rabbit. The targeting transducer was the Diasonics endocavitary probe.
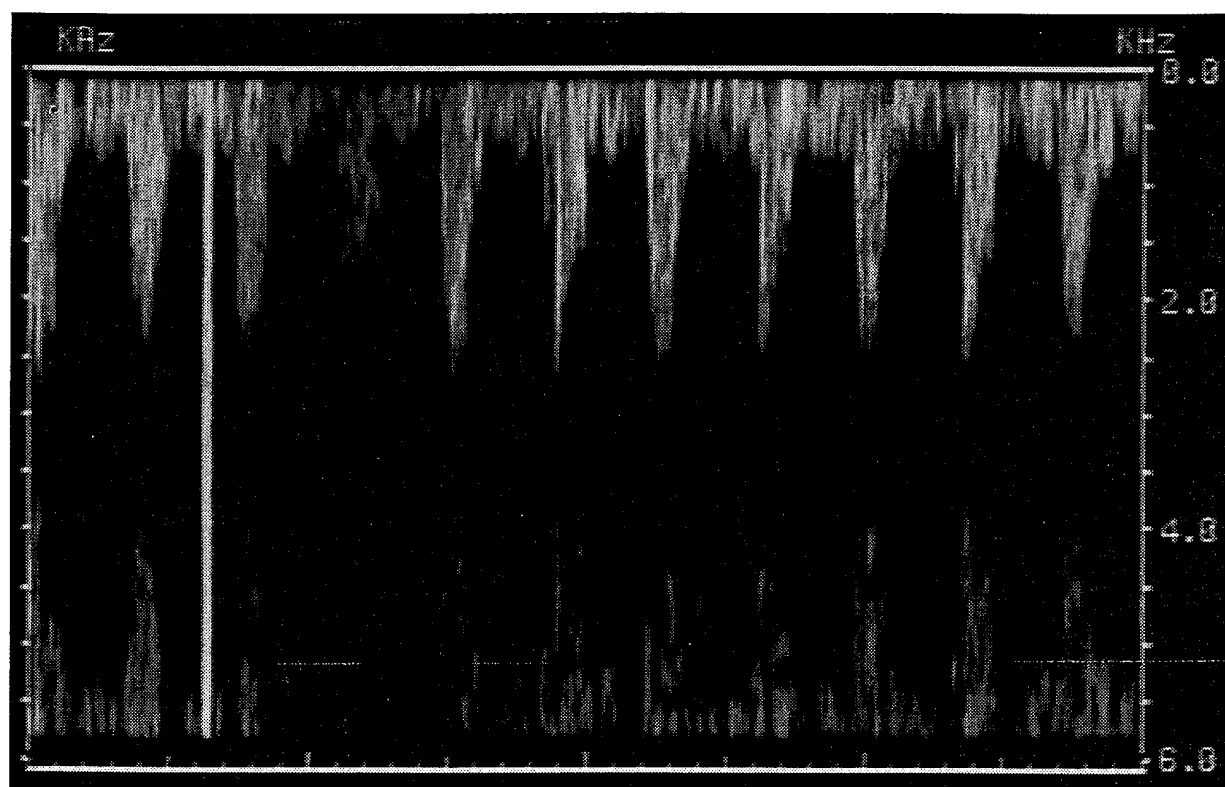
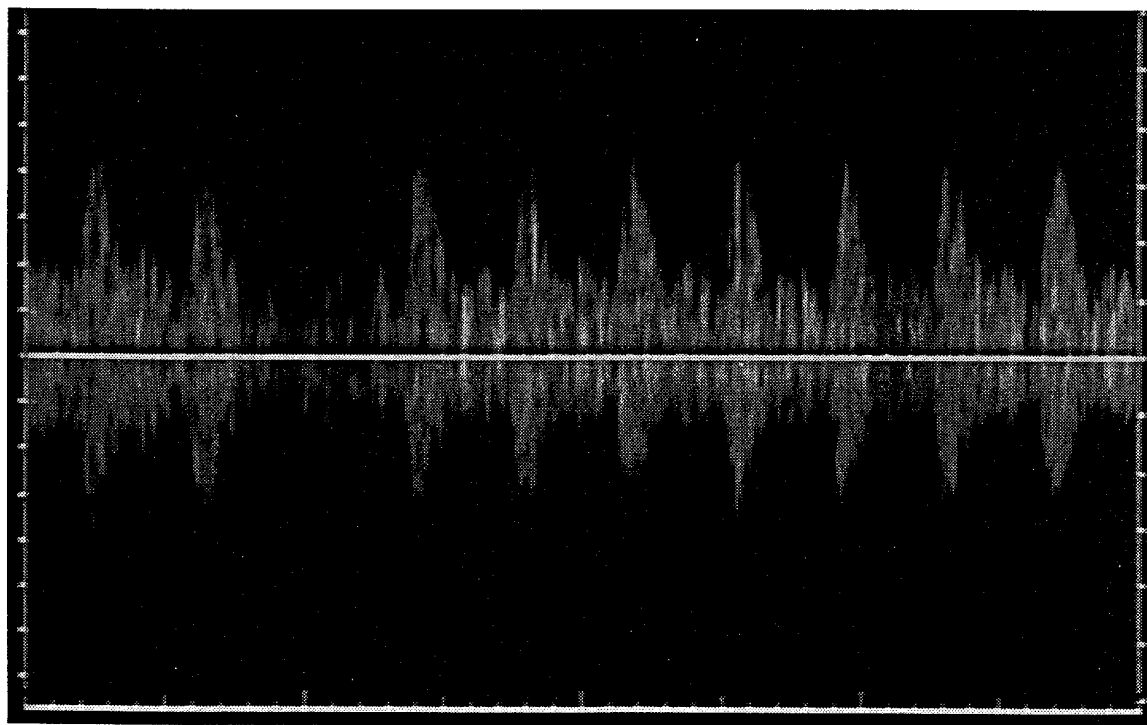Figure 3 - Example of transcutaneous contrast interruption *in vivo* using 20 msec burst.

Figure 4 - Example of transcutaneous contrast interruption *in vivo* using 80 cycle (~40 μsec) burst.

· A series of contrast injection were performed while varying amplitude and burst length of the contrast interruption field. Figure 3 shows an example of the result for a 20 msec burst at approximately 20 MPa. After the second peak systolic portion of cardiac waveform, a large vertical band is seen. This is an interference artifact from the firing of the high power transducer. During the third cardiac cycle, an abrupt decrease in the brightness of the Doppler spectral display is seen. The amplitude of the display had been set so as not to saturate in the presence of the ultrasound contrast agent. Therefore the decrease that is seen is down to the level of the pre-contrast signal coming from blood. Note that the decrease comes after the interference effect owing to the transit time for the negative bolus produced in the femoral artery upstream. What was extraordinary was that burst length could be reduced to as low as 40 cycle (~20 μsec) and the effect could still be seen from a single application. Figure 4 is the result for an 80 cycle (~40 μsec) burst. Note that this time the interference from the firing of the high power transducer is not seen because it was so short on this time scale. However, the decrease in Doppler signal strength is present again lasting approximately 1 cardiac cycle. This is consistent with the possibility that the shorter pulse is sufficient to create the negative bolus in the femoral artery and this bolus is swept downstream with the next cardiac cycle. The cardiac cycle duration would perhaps ultimately control the duration of the negative bolus.

As part of another project exploring the use of high power ultrasound to transcutaneously generate bubble *in vivo* , we were also able to perform a single canine experiment to further investigate contrast interruption. The experimental protocol was essentially the same as that above with the following exceptions. The acute animal was initially anesthetized with suritol (3mg/kg), intubated and anesthesia maintained by ventilation with 3% enflurane. The contrast interruption was monitored in the femoral artery immediately downstream from the interruption site. As the animal had no carcinoma in the thigh, the site selected was based on the constraints of the other experiments being performed. Because of the proximity of the contrast interruption to the observation site it was difficult to detect the negative contrast bolus, however, there was some indication from observations during the experiment that contrast flow was being disrupted. Further examination of the data has not yet been performed to confirm these observations but should be available at a later writing.

In addition to these specific advances in contrast interruption, research arrangements with Diasonics Ultrasound have resulted in some techniques which we will be able to apply in the coming year. Harmonic imaging is now available on the Diasonics Spectra which will should provide improved signal to clutter noise ratios for this research. Harmonic imaging uses the B-mode or Doppler imaging modes of the scanner to transmit at one frequency and receive at harmonics of that frequency. The response of bubbles at the second harmonic of the driving frequency provides signal strength which is orders of magnitude greater than that coming from tissue. Through this project and a subcontract to an NIH SBIR subcontract we have measured second harmonic emissions from a number of contrast agents, including MRX-115. Figure 5 is a power mode image of a canine kidney *in vivo* before and after injection of the MRX-115. The dramatic signal increase in the imaging mode as the agent passes through indicates that this agent should provide excellent interruption capabilities for regional perfusion estimates. Experiments are now underway to test the enhancement seen in the second harmonic mode. Our initial measurements of the second harmonic emission indicate that the agent should provide reasonable second harmonic emission as seen in Fig. 6 where the second harmonic is only 20 dB below the fundamental.
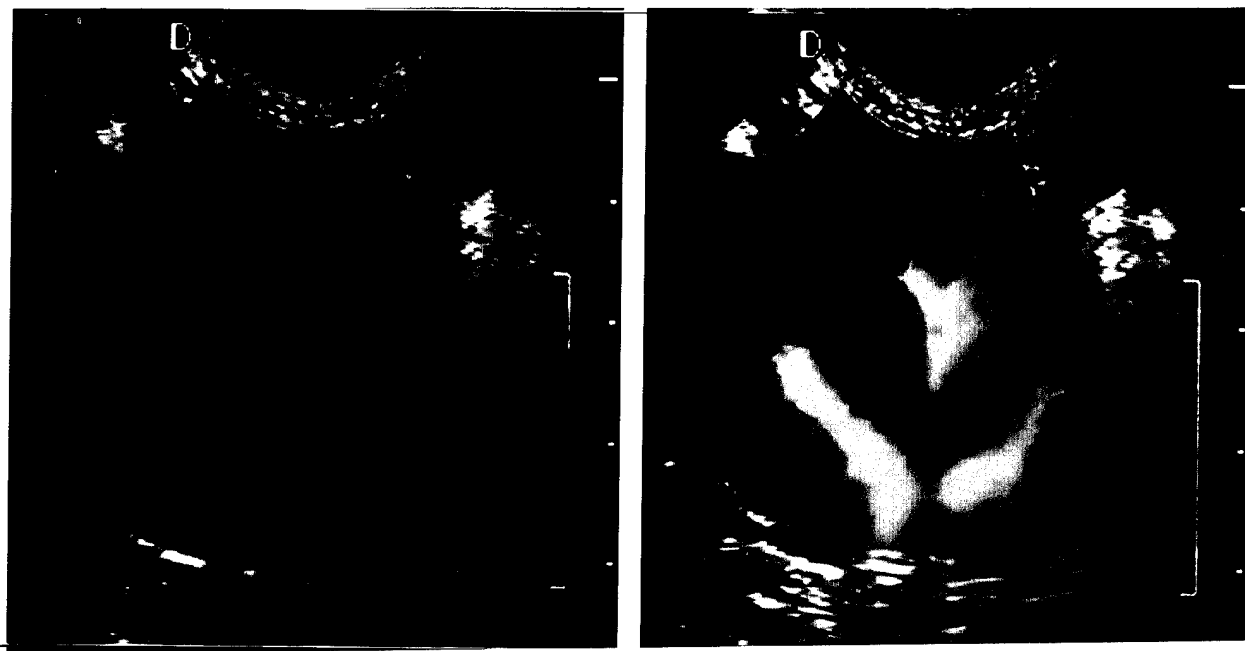
Figure 5 - Power mode image of a canine kidney before (left) and after (right) IV injection of MRX-115 contrast agent.
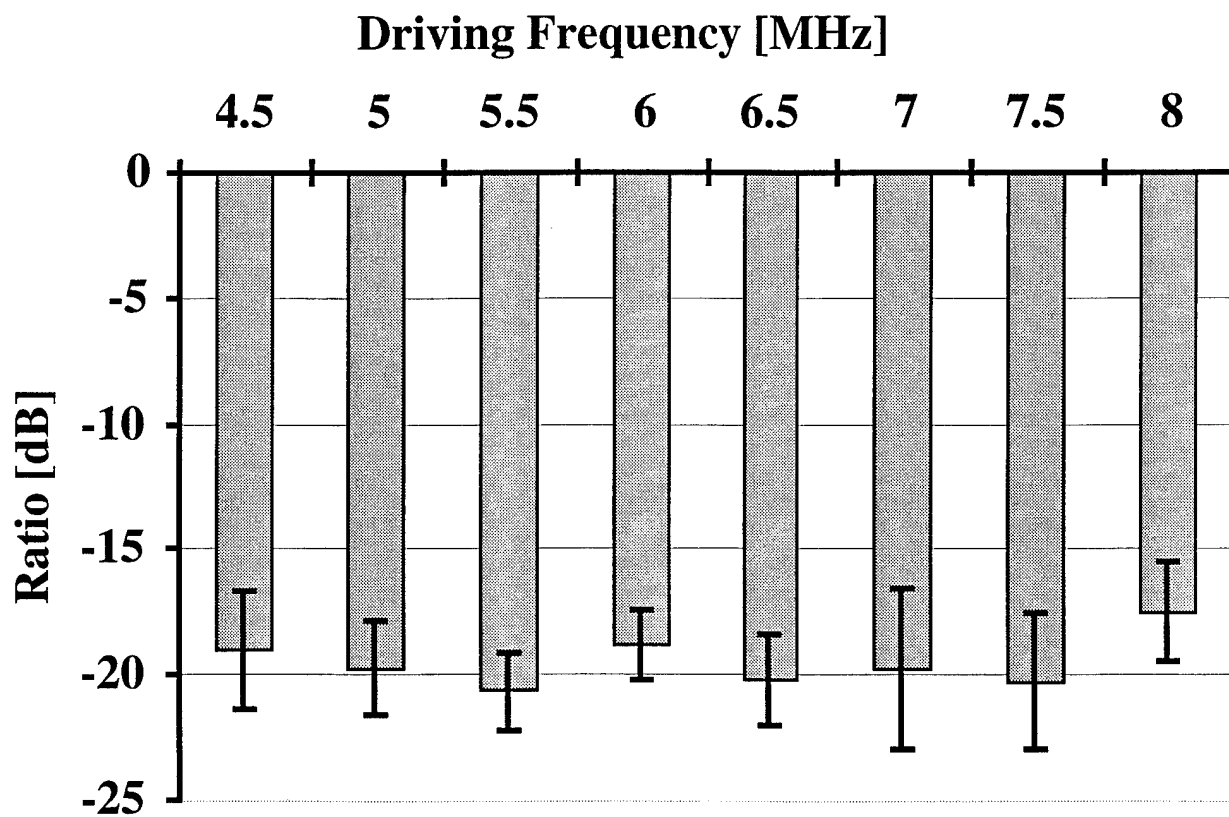

Figure 6 - Second harmonic signal amplitude relative to the fundamental as a function of the driving signal frequency.

These results for both the leporine and canine experiment can now be used as guides for *ex vivo* experiments. The indication is that shorter than anticipated burst may be effective in contrast interruption and time with the cardiac cycle may indeed be important. Most importantly, these experiments have clearly indicated that contrast interruption can be performed <u>transcutaneously</u>, improving the chances of success for this project. This sets the stage for the more extensive 2nd year evaluations in animal studies.

Decorrelation Techniques and Combination Blood Flow Measurements

The manuscript concerning decorrelation techniques for perfusion estimates, a significant part of the original proposal, has been refined during the course of this past year and has now been published. Attached is a copy of the publication for that work. Further direct progress in this area has been delayed to some degree by a transition in the hardware of the Diasonics Spectra VST which defeated our software as originally implemented on the scanner. The research platform has now stabilized and we are in the process of implementing that software again. Two improvements in our situation with regard to this software have occurred recently. The first is that the new Diasonics platform has a removable hard disk drive which will make the storage and transfer of data more convenient and also ease the transfer of new software such as our decorrelation code. Secondly, during this downtime we have made what may be a significant use of the decorrelation idea in another area which impacts the technique which combines Doppler power and velocity data. As was indicated in our original proposal, this work is being performed in conjunction with that of Dr. Paul Carson on 3D breast imaging. Even though 3D imaging is not a specific part of this grant, the idea was to utilize the same data acquisition system so comparison could be made between techniques. In the course of conversations concerning the difficulties associated with breast scanning, it was suggested that the elimination of encoding hardware would be desirable and helpful in terms of examining images acquired from a variety of scanners. It was suggested that one might be able to use the decorrelation of signal in the elevational direction to determine the separation between slices which were obtained using a manual scan. The following is a description of the techniques which is taken from a preliminary patent application.

The approach being taken by most ultrasound companies is to build a (usually hand-held) motorized scan head specifically for 3-D imaging. This approach has a disadvantage of high cost, low reliability and limitation on the number of scan heads available for 3-D. Often coupling paths are employed with their inherent attenuation and reverberation problems. Also, the scan rate for optimal color flow imaging is a complex function of all the Doppler time constants, frame rate and the particular vascular signal levels. In regular imaging with a given scan head, the operator or observing radiologist might want to capture in 3-D images observed with a particular scanner using an arcing or linear sweep. If relative 3-D image position can be obtained by processing the series of images or data used to produce the images, a great new flexibility and efficiency will be achieve. Major 3-D capabilities will only be required on a central workstation which can record a single series of images and display them in their proper position in a stacked slice 3-D display. The radiologist, technologist at the scanner, or other trained observer will view the slices sequentially in their proper position on the display. They will select the most appropriate 2, 3 or 4-D display method and views to demonstrate the noted information in the most informative way for surgeons and other referring physicians or to obtain the desired quantitative measurements.

Correlation techniques have been used extensively to estimate tissue motion in applications such as blood flow (Adler, Rubin et al. 1995, Appendix 1) and imaging tissue elastic properties (Adler, Rubin et al. 1990; Ophir, Cespedes et al. 1991; Chen, Jenkins et al. 1992; O'Donnell, Skovoroda et al. 1994). Some commercial ultrasound systems now use correlative algorithms for their color flow imaging rather than various forms of Doppler processing. We are suggesting the use of correlation to perform the opposite task namely assume the tissue to be stationary and track the movement of the transducer. Trahey *et al* (1986) used correlation of speckle to determine the amount of lateral translation of a phased array required to achieve statistically independent information for speckle reduction by image compounding. Their experimental results show correlation curves as a function of translation distance which are smoothly varying, suggesting that

measuring the rate of decorrelation and knowing the point spread function for the aperture, one can use the same speckle statistics to estimate the actual transducer motion. The correlation techniques which we have developed provide the mechanism for slice positioning and involve the adaptation of some software already developed.

In order to test the concept of image-based slice positioning, images of a rather inhomogeneous contrast detail phantom were made. In all cases the images were post-processing in a modular code under the AVS software package of Advanced Visualization Systems. A full description of the mathematical process is given in the attached manuscripts of Chen *et al.*. Images were collected from an ultrasound scanner and read into the workstation memory. The RGB images are then processed to select one channel for B-mode and then the 3-D data set is sliced and a single 2-D plane displayed to select regions of interest (ROIs) to be processed for determining the slice separation. The pixels contained in the ROI in each image are converted to a 1D vector and the process repeated for each image. Each of these vectors are then combined in a 2-D vector. These data are then subsampled to determine the how many of the image ROIs will be used to compute the position of each image. The group of image ROIs is then analyzed to compute the correlation between successive ROIs, i.e. ROI#1 correlation to ROI#2, ROI#2 to ROI#3, etc. for a one step correlation value. The process is repeated for two, three, etc. step correlations. For the hand-scanned images, ROIs from groups of ten images were used to determine the slice separation for the center two slices, e.g., to position image 6 with respect to 5 use information from images 0-9, for image 7 after 6 use image 1-10, etc. This does assume a piece-wise smooth motion for the scanhead, which should be achievable and is necessary for any good continuous power mode imaging. In each case, the correlation curve was fit using a least squares approach to the Gaussian functiongiving the relationship between step size, point spread function and correlation value. This information is then used to position the images appropriately in space for further display.

Two sets of images were obtained in the initial trial. A measured correlation curve was first determined for mechanical stepping with the breast scanner using a 3.5 MHz curved linear array. Using several regions of interest at the same depth range and a least squares method for a Gaussian curve-fitting, the step size was estimated for several regions of interest to be $\delta y = 0.17 \pm 0.02$ mm, compared to the actual step size used of 0.175 mm. In this case the decorrelation curve was measured across a number of images where it could be assumed that the step size was constant for the mechanical stepping. A hand scan was then performed where images at 32 fps were stored in a 120 frame cine loop. Results given in Fig. 7 show the appearance of the echogenic cone is not very different for this short scan when using either an equal slice separation assuming uniform hand scanning rate or that calculated using the image decorrelation rate. However, the lower graphs illustrate the decorrelation does track smoothly the nonuniform motion of the slow, hand scanning currently used for 3-D power mode imaging. Black stripes in the subtraction image correspond to zeros in the integral displacement error of the uniform stepping as plotted in the graph on the right.

These techniques can be used to correct positioning errors for hand-scanned image acquisitions in the breast. This could have an important impact in the research being performed here since regional perfusion measurements will rely on know the position of the scanhead when combining Doppler power and velocity information together as an estimate of perfusion. The image-based slice positioning techniques will allow more examinations to be performed in some of the more interesting cases, i.e. the smaller dense breast which is a particular difficulty in mammography.
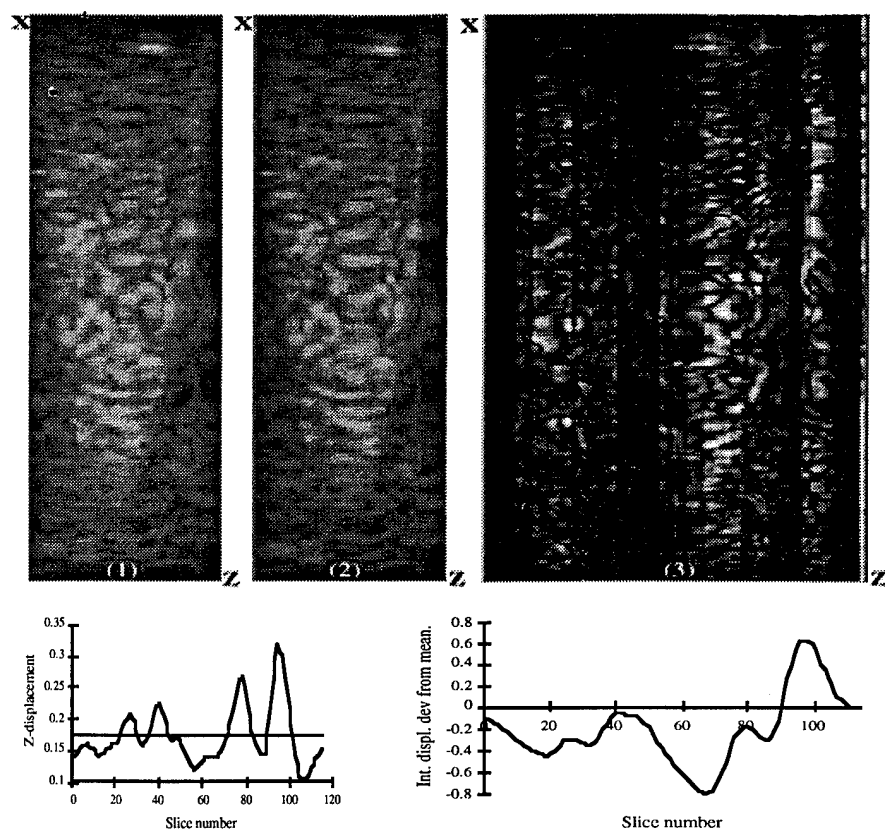
Figure 7 - Left to right top images: 1) C-scan, longitudinal view of a cone object from a hand-scanned, 3.5 MHz, curved linear array assuming equal step size; 2) The same view with actual step size as estimated by the speckle decorrelation; 3) The subtraction between these two views (expanded horizontally). For comparison, image 1 was scaled to the same lateral size as image 2. The left graph below shows the step size change with step number as calculated from the decorrelation, while the right graph shows the integrated displacement change with step number.

CONCLUSIONS

The results of the research thus far indicates that contrast interruption is possible *in vivo* using acoustic fields and such interruption results in a negative contrast bolus which is well resolved in time. Accomplishing the transcutaneous interruption of contrast further defines the circumstances which are relevant to use in a more complete study of the process *in vitro*. These studies should allow us to reduce the acoustic amplitude required to generate the bolus and to control the time course of the interruption.

The development of image-based slice positioning should provide a more accurate assessment of the tissue perfusion using the estimation techniques proposed in this research. Perhaps equally important is the potential for these techniques to have an impact on the overall use of 3D ultrasound to map the breast vasculature. Therefore although this was not a specific goal of this research, the significance of this work may reach beyond the concept originally proposed in terms of decorrelation measures and the combination of Doppler power and velocity information to estimate perfusion.

REFERENCES

Adler DD, Carson PL, Rubin JM (1988) Evaluation of Doppler ultrasound flow imaging in the diagnosis of breast cancer. Procs.World Federation Ultras. in Med. and Biol., Oct. 17-21, J. Ultrasound Med, **7**, S271, abstract only.

Adler DD, Helvie MA and Ikeda DM (1990) Follow-up strategies for marginally suspicious nonpalpable breast lesions, Amer. J. Roentgenol., in press.

Adler, R. S., J. M. Rubin, et al. (1989). "Characterization of transmitted motion in fetal lung: Quantitative analysis." Med. Physics 16(3): 333-337.

Axtel LM, Asire AJ, and Meyer MH (eds) (1976) Cancer patient survival. Report #5. DHEW Pub. No. (NIH) 77-992, Bethesda MD, NCI.

Boyd J. Jellins J, Reeve TS, and Kossoff G. (1983) Doppler Examination of the Breast *in* Ultrasound Examination of the Breast. Ed, J. Jellins and P. Kobayashi, John Wiley and Sons, New York, 386.

Burns PN, Halliwell M, and Wells PNT (1982) Ultrasonic Doppler studies of the breast. Ultrasound in Med. and Biol. 8, 127.

Chang CHJ et al (1982) Computed tomographic mammography using a conventional bodyscanner. Am. J. Reont. 138, 553.

Chen, E. (1992). Uncertainty in Estimating Tissue Motion from Ultrasonic Images. Department of Electrical and Computer Engineering, University of Illinois, Urbana, IL.

Cosgrove DO, Bamber JC, Davey JB, McKinna JA and Sinnett HD (1990) Color Doppler signals from breast tumors, Work in progress. Radiology, 175-180.

Feldman F et al. (1967) Arteriography of the breast. Radiology 89, 1053.

Flynn MJ, et al. (1984) Digital Subtraction Angiography Techniques for the Evaluation of Breast Lesions. Park Press, SPIE Vol. 468, 129.

Harms, et al. (1993) MR imaging of the breast with rotating delivery of excitation off resonance: clinical experience with pathological correlation. Radiology, 187, 493-501.

Heywang-Kobrunner SH, Haustein J, Beck R, et al. (1992) Contrast -enhanced MR imaging of the breast: influence of dose of Gd-DTPA. Radiology, 185(P): 245.

Horak ER, Leek R, Klenk N, LeJeune S, Smith K, et al. (1992) Angiogenesis, Assessed by Platelet/Endothelial Cell Adhesion Molecule Antibodies, as an indicator of Node Metastasese End Survival in Breast Cancer, Lancet, 340, 1120-1124.

Ivey JA, Gardner EA, **Fowlkes JB**, Rubin JM, Carson PL: Acoustic Generation of Intraarterial Contrast Boluses, Ultrasound Med. Biol., accepted, 1995.

Jellins J (1988) Combining imaging and vascularity assessment of breast lesions, Ultras. Med. & Biol., 14, Sup 1, 121-130.

Kaushik SP, Desle BY, Sodhi JS (1975) Breast angiography and clinico-pathological correlation in breast tumours. Indian J. Cancer, 367.

Minasian H and Bamber J (1982) A preliminary assessment of an ultrasonic Doppler method for the study of blood flow in human breast cancer. Ultrasound in Med. and Biol. 8, 357.

Moskowitz M, and Gartside PS (1982) Evidence of breast cancer mortality reduction, aggressive screening in women under age 50. AJR 138, 911-916.

O'Donnell, M., A. Skovoroda, et al. (1994). "Internal displacement and strain imaging using ultrasound speckle tracking." IEEE Trans. Ultras. Ferroelect. Freq. Control 41: 314-325.

Ophir, J., I. Cespedes, et al. (1991). "Elastography: a quantitative method for imaging the elasticity of biological tissues." Ultrasonic Imag. 13: 111-134.

Rubin JM, Carson PL, Zlotecki RA, and Ensminger WD (1987) Visualization of tumor vascularity in a rabbit VX2 carcinoma by Doppler flow mapping. J. Ultrasound Med. 6, 113.

Sakki S (1974) Angiography of the female breast. Ann. Clin. Res. 6, Suppl. 12, 1.

Trahey, G., E (1986). "Speckle Pattern Correlation with Lateral Aperture Translation: Experimental Results and Implications for Spatial Compounding." IEEE Trans. on Ultra. Ferroelectrics, Frequency Control UFFC-33(3): 257-264.

Weidner N, Semple JP, Welch WR, Folkman J (1991) Tumor Angiogenesis and Metastasis Correlation in Invasive Breast Carcinoma, The New England Journal of Medicine, Vol. 324, No. 1.

APPENDICES

Adler RS, Rubin JM, Fowlkes JB, Carson PL, Pallister JE: Ultrasonic Estimation of Tissue Perfusion: A Stochastic Approach, Ultrasound Med. Biol. Vol. 21 (4), 493-500, 1995.

Chen, et al. Determination of Scan Plane Motion Using Speckle Decorrelation. (To be submitted to JASA)

Pergamon

0301-5629(94)00135-9

●*Original Contribution*

ULTRASONIC ESTIMATION OF TISSUE PERFUSION: A STOCHASTIC APPROACH

RONALD S. ADLER, JONATHAN M. RUBIN, J. BRIAN FOWLKES,
PAUL L. CARSON and JOHN E. PALLISTER

University of Michigan Medical Center, Department of Radiology, Ann Arbor, MI, USA

Abstract—Imaging of blood flow perfusion is an area of significant medical interest. Recently, the advantages of using the total integrated Doppler power spectrum as the parameter that is encoded in color has been shown to result in an approximately threefold increase in flow sensitivity, a relative insensitivity to acquisition angle and lack of aliasing. We have taken this mode a step further and demonstrated the potential for quantifying blood flow using correlation-based algorithms applied to the power signal. We show that $\Phi(\tau) = \Phi(0)e^{-\nu\tau}$, $\tau > 0$, where $\Phi(\tau)$ is the two-time correlation of the fluctuation in the power signal, and ν is the specific flow (reciprocal of mean transit time). Scans of a dog's blood, pumped at a constant rate through gum rubber tubing, were obtained using a Diasonics Spectra 10-MHz linear array transducer at standard range-gated spectral mode (PRF = 1400 Hz, wall filter = 50 Hz, sample gate = 1.5 mm). A fixed Doppler angle of 68° was used. Five different flow rates were tested, and the velocities determined by power decorrelation were compared to the mean velocities calculated from the Doppler shifts by linear regression ($R^2 = 0.987$). We believe the results are very encouraging for using power decorrelation in perfusion evaluation.

Key Words: Decorrelation, Power Doppler, Ultrasound.

INTRODUCTION

A variety of physiological processes, reflecting both normal and pathologic states, can be characterized by a relative increase in local soft tissue perfusion, soft tissue inflammation being an example. It is not surprising, therefore, that there has been considerable interest and expense devoted to producing quantitative maps of such information. Technological improvements in ultrasound imaging during the past 5 years or so have shown this modality to be capable of depicting blood flow without the need to administer intravascular contrast agents, although flow sensitivity is clearly improved when such agents are utilized. Doppler ultrasound, using mean frequency maps, is a well-developed and commercially available technique which can noninvasively depict flow in large vessels, provided adequate acoustic access exists. Alternatively, the relatively poor signal-to-noise characteristics of mean-frequency maps has limited this application as a means to fully and inexpensively assess many abnormal flow states commonly encountered in medical practice.

The development of a more sensitive ultrasonic measurement of blood flow has been proposed by Dymling et al. (1991) in which the first frequency moment of the backscattered power spectrum has been shown to provide an estimate of flow in a randomly oriented microvascular bed. This latter property allows one to derive an explicit relationship between the first moment and the local tissue perfusion. It is not yet clear, however, as to the general validity of these assumptions regarding the morphologic nature of the capillaries in most tissues. Alternatively, the integrated power spectrum is available on many ultrasonic imagers and, as these authors point out, this measurement is directly proportional to the total number of scatterers in the insonified volume (Dymling et al. 1991). The nature of this proportionality may be quite complex, however, being influenced by such things as attenuation, beam pattern, Doppler wall filter, clutter cancellation and frequency (Eriksson et al. 1991; Mo and Cobbold 1992).

Rubin et al. (1994) have demonstrated the utility

Address correspondence to: Ronald S. Adler, Ph.D., M.D., University of Michigan Medical Center, Department of Radiology, 1500 E. Medical Center Drive, Ann Arbor, MI 48109-0030, USA.

of color-encoded maps of integrated power on two commercially available systems, referring to it as power Doppler imaging and, more importantly, they have demonstrated a significant improvement in signal-to-noise, relative to mean-frequency maps, in depicting flow. One example consists of displaying the soft-tissue blush in the renal cortex, which typically requires administration of an intravascular contrast agent. This particular feature is currently being made commercially available by a number of ultrasound vendors as a means of increasing flow sensitivity and more accurately representing vessel morphology.

Inherent limitations of power Doppler, besides its significant motion sensitivity, relate to more fundamental issues. An estimate of the total number of moving scatterers is being displayed rather than the more physiologically relevant parameter, the blood flow itself. The total power displayed is not entirely velocity independent due to the effects of the soft-tissue clutter canceler, which modulates the amplitude of low velocity components, thereby introducing a frequency dependence. Despite this limitation, we show, in the current work, that the inherent stochastic nature of such estimates, prior to any temporal filtering (i.e., persistence), can provide additional information. Such estimates have been made in the past based on pure statistical fluctuations in either pressure amplitude in A lines or envelope variations from backscattered ultrasound (Atkinson and Berry 1974) and using scattering theory arguments applied to a Doppler signal (Mo and Cobbold 1992). In our case, we will estimate local tissue perfusion from the nontemporally averaged data by solving a stochastic differential equation derived from a flow model with noise. Similar relationships are well-known from linear response theory and relate the fluctuations that drive a system to the systematic response of the system (i.e., a transport coefficient in the case of hydrodynamic phenomena) via the fluctuation dissipation theorem (Mori and Fujisaka 1973; Papoulis 1965; Zwanzig 1960). Inasmuch as such a mathematical approach to local biologic phenomena is not particularly well-known, the relevant theoretical considerations are developed in some detail below. It is shown that the rate of decorrelation within a region-of-interest directly relates to specific flow, as suggested below. To illustrate the technique, a simple flow phantom under conditions of constant input is studied. Mean velocity (proportional to flow in this geometry) is directly compared to estimated velocity based on known sample volume and estimated transit time obtained from decorrelation.

THEORY

The principal assumption in power Doppler imaging pertains to the direct relationship between total power within a voxel (or region of interest) and the mean number of scatterers within that voxel. This relationship holds provided that multiple scattering events are negligible for the range of fractional blood volumes considered, and the flow is not turbulent. Typically power Doppler images are displayed with large amounts of temporal averaging with different frame weightings to diminish the effects of soft tissue motion (Rubin et al. 1994). Such maneuvers diminish the statistical fluctuations in the power display. To restore these fluctuations, the temporal averaging is removed. Thus, for each frame within the nontemporally averaged "power" image, a number N is derived, representing the instantaneous estimate of the number of scatterers entering the tissue volume, V, per unit time. This number, in general, is subject to some variation from frame-to-frame due to inherent noise in the rate of scattering, as well as the acquisition and signal processing system itself. These factors include attenuation and beam geometry as mentioned earlier. However, the final specific flow is obtained from a normalized expression, canceling many of these effects. A stochastic equation is derived which contains information related to the rate at which scatterers enter the voxel, provided that certain specific assumptions are valid (see below). For simplicity, we consider a constant input.

We suppose that the input flow is not random and depends only on the number of scatterers (RBCs in this case) and flow per unit mass, F. In general, since the instantaneous estimate of N is subject to noise, the actual and estimated inputs are not equivalent. To describe the time dependence of this random variable, therefore, it is necessary to write an appropriate stochastic differential equation. In this case we assume the simple form:

$$dN/dt = F(C_A - mN/V) + f(t) \qquad (1)$$

where m = mass per scatterer, F = flow per unit mass, V = volume of interest, N = instantaneous number of scatterers in V, $f(t)$ = stochastic driving force, C_A = arterial mass concentration of scatterers.

The time rate of change in N depends on the systematic term (i.e., due to flow) and a noise term, $f(t)$, characterizing the stochastic nature of the system. This so-called Langevin equation is well-known within the statistical mechanics literature (Mori and Fujisaka 1973; Papoulis 1965). Several formal properties of this relation may be derived; these may be regarded as a subset of the more general Langevin approach (Mori and Fujisaka 1973). Upon averaging eqn (1) over all realizations of N, recognizing that under steady flow conditions $\langle N \rangle$ is constant, results in

$$d\langle N \rangle/dt = 0. \qquad (2)$$

Further, by conservation of mass:

$$FC_A = Fm\langle N \rangle/V$$

or

$$\langle N \rangle = C_A V/m, \qquad (3)$$

The mean number of scatterers contributing to the power image reflects mean transport of RBCs into V. From eqs (1) and (3), it follows that:

$$\langle f(t) \rangle = 0. \qquad (4)$$

The fluctuation in N

$$\delta N = N - \langle N \rangle \qquad (5)$$

satisfies a somewhat simplified expression

$$\frac{d\delta N}{dt} = -\frac{mF}{V}\delta N + f(t) = -\nu\delta N + f(t) \qquad (6)$$

where

$$\nu = mF/V = \text{specific flow.} \qquad (7)$$

The remaining points to consider deal specifically with the statistical properties of this system. For this purpose, a new function is introduced

$$\Phi(\tau) = \langle \delta N(t + \tau)\delta N(t) \rangle \qquad (8)$$

which is the two-time correlation function for the expected number of scatterers in V. Three additional properties must first be developed. Stationarity is already inherent in eqn (8) and indicates the independence of $\Phi(\tau)$ on the initial time t. The second property, termed causality, indicates that $f(t)$ and $\delta N(t')$ are not correlated when $t' < t$. The final statement refers to the basic Markov nature of eqn (6), which when combined with the assumption of stationarity, results in the so-called fluctuation dissipation theorem:

$$\langle f(t)f(t') \rangle = \sigma\delta(t - t') \qquad (9)$$

in which it is apparent that $f(t)$ is a white noise process and σ is a constant. In terms of these assumptions, a simple expression for $\Phi(\tau)$ will be derived. Solution of eqn (6) results in

$$\delta N(t) = e^{-\nu t}\delta N(0) + \int_0^t d\tau e^{-\nu(\tau-t)}f(\tau) \qquad (10)$$

which, after forming $\Phi(\tau) = \langle \delta N(t + \tau)\delta N(t) \rangle$, results in

$$\Phi(\tau) = [\Phi(0) - \sigma/2\nu]e^{-\nu(t+t')} + \Phi(0)e^{-\nu|t-t'|} \qquad (11)$$

in which $|\ |$ denotes absolute value. For stationarity to be satisfied, we require that

$$\sigma = 2\nu\Phi(0) \qquad (12)$$

so that eqn (11) simplifies to

$$\Phi(\tau) = \Phi(0)e^{-\nu\tau}, \quad \tau > 0 \qquad (13)$$

which is to say that the decay of the correlation function itself gives an estimate of the specific flow.

EXPERIMENTAL METHODS

Experiment 1

Preliminary experiments were performed to test the accuracy of the decorrelation method in the measurement of perfusion. In a simple flow experiment, gum rubber tubing with an internal diameter 1 cm was positioned so that the angle of incidence was 0° between the flow stream and imaging field of a Diasonics Spectra VST using a 10-MHz probe. This geometry maximized the Doppler frequency shift for any flow velocity. The flowing media was a mixture of corn starch (2 g/L) in water circulated by a peristaltic pump with the fluid reservoir acting as a capacitance chamber to produce a constant flow of 10 to 20 mL/min through the tube. Knowing the size of the pixels used in displaying the power mode color and the input volume flow rate to the tube, it was estimated, assuming a parabolic velocity profile across the tube, how rapidly each pixel would have to be sampled to observe the decorrelation time at various positions within the tube. The rate at which the power color display is updated at any given pixel corresponded to the frame rate of the ultrasound imager. At this rate, all but the slowest flows essentially decorrelated instantly. To lengthen the decorrelation time, effective pixel size was increased by summing pixels along the direction of flow and using the total power in these pixels as if they represented one sampling site. Hence, the total power in n contiguous pixels along the flow direction effectively lengthens the region-of-interest and permits measurement of decorrelation rates that are n times faster than before (*i.e.*, the transit time is increased by a factor of n).

Using software made available by Diasonics for experimental use on their Spectra machine, a buffer is filled with sequential frames of nontemporally averaged power mode data. This data is then descrambled and loaded into an image processing software package (Application Visualization System [AVS]) in the form of a three-dimensional (3D) (2 spatial, 1 temporal) scalar byte field. Each byte represents a decibel-scale value of the Doppler signal amplitude at that location.

For each set of data, a region of interest is selected within an area of constant flow, i.e., a specified distance from the center of the tube. The pixels within this region are written to one line of a two-dimensional (2D) field. Each line of this field is sequentially filled from the same ROI (region-of-interest) of each frame in the original 3D field.

Each point in this field is then converted to a linear scale and the global mean is subtracted.

$$P(x, t) = 10^{I(x,t)/106.67} - \frac{1}{M} \sum_{m=0}^{M-1} 10^{I(x,m)/106.67}$$

where $P(x, t)$ is the linear zero mean power value, $I(x, t)$ is the raw decibel data, M is the number of frames and L is the size of the ROI minus $j - 1$, where j is the number of pixels summed along the flow direction to "lengthen" a pixel. The factor 106.67 is used to convert the 0 to 255 log scale for intensity to a linear scale.

The correlation is then calculated using the expression

$$\text{corr } (m) = \frac{1}{M - m} \sum_{n=0}^{M-m-1} \sum_{l=0}^{L-1} P(l, n) \times P(l, n + m)$$

where corr (m) is the time correlation between ROIs, and m is the frame separation.

The normalized correlation is:

$$\text{Corr } (m) = \frac{\text{corr } (m)}{\text{corr } (0)} .$$

Experiment 2

In a second experiment, the spectral Doppler mode was used to obtain data at a much faster rate than was possible in the power mode. This allowed measurement of faster flows where the Doppler shift was more easily detected in addition to the greater flow sensitivity of the spectra Doppler mode itself. In this case, fresh canine blood was used as the flowing medium through a length of 0.6-cm-diameter dialysis tubing. The pumping system was unchanged and the Doppler spectral data was acquired from the center of the tube using a fixed angle of 68° at various flow velocities as measured from the Doppler spectrum. To analyze the spectral data, the digital data was again dumped from the Diasonics Spectra and analyzed using AVS. The analysis consisted of converting the digital values coded in 8 bits to the 42-dB dynamic range of the Doppler spectrum. In general, spectral Doppler data consists of a series of power spectra which are acquired at each time step and encoded in pixel intensity. Therefore, at each time point in the data, the corresponding power spectrum was integrated to yield the same result for the single Doppler sample volume as is encoded in color at each pixel in the power mode image. The sampling interval, corresponding to the time windows over which individual fast-Fourier transforms were performed, is about 2 ms. This is about 50 times faster than the frame rate in the color mode, typically about 10 frames/s. The integrated power was then windowed and an autocorrelation performed with the mean subtracted. The decorrelation results were then used to compute the rate at which the blood was flowing through the Doppler sample volume, and this result was compared to the mean flow velocity as measured using the angle corrected Doppler frequency shift according to

$$\bar{f} = \frac{\int fP(f)df}{\int P(f)df}$$

where $P(f)$ is the Doppler power spectrum and f is the mean frequency shift.

RESULTS

Experiment 1

Figure 1a depicts the decorrelation within the tube flow at two locations. Assuming laminar flow, which is appropriate for these flow rates, the decorrelation is faster in the center of the tube than near the walls, as expected. Using the ROI near the tube wall, the number of pixels treated as a single sample region was varied and the effect of this is presented in Fig. 1b. As the number of pixels is increased, effectively lengthening the ROI, the decorrelation time increases. This is consistent with the notion that the fluid flowing through this enlarged region would take a long period of time to pass.

Experiment 2

Using the spectral Doppler data, the results are similar to those obtained by the power mode imaging.
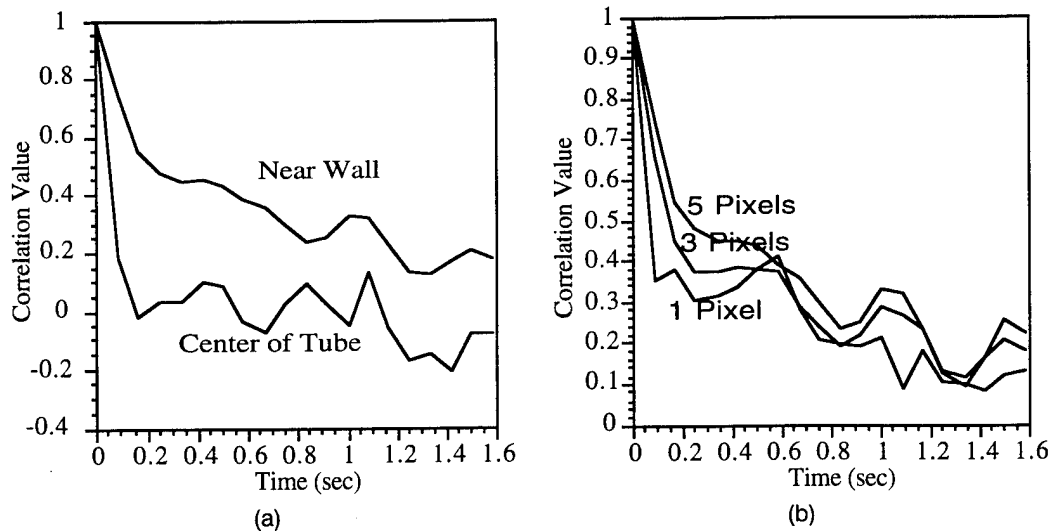
Fig. 1. Results taken using the power mode decorrelation technique in the tube flow system. In this case, the tube was positioned such that the flow was directly toward the transducer. Therefore, pixels could be averaged along the flow direction (see Methods). The pixel number indicates the number of pixels used in the average. (a) The data indicates the effect on the decorrelation rate for the increased flow in the center of the vessel compared to the flow near the walls. (b) A comparison of the effect of the number of pixels used in the average.

An example of the integrated power spectra versus time is given in Fig. 2a. Note the quasiperiodicity in the integrated power related to the speckle pattern of the finite aperture used in the ultrasound imaging. Figure 2b is a plot of the decorrelation-calculated flow velocity versus the flow velocity as measured by the Doppler frequency shift. The conversion of the decor-relation time to a velocity is based on the transit of the Doppler sample volume in the direction of the flow and the time for decorrelation to 0.5. The slope of the linear fit is 0.91 with an $R^2 = 0.98$ indicating nearly a one-to-one correspondence for the measured velocities. The intercept for the fit is 0.69 mm/s, which indicates the movement of blood in and out of the Doppler
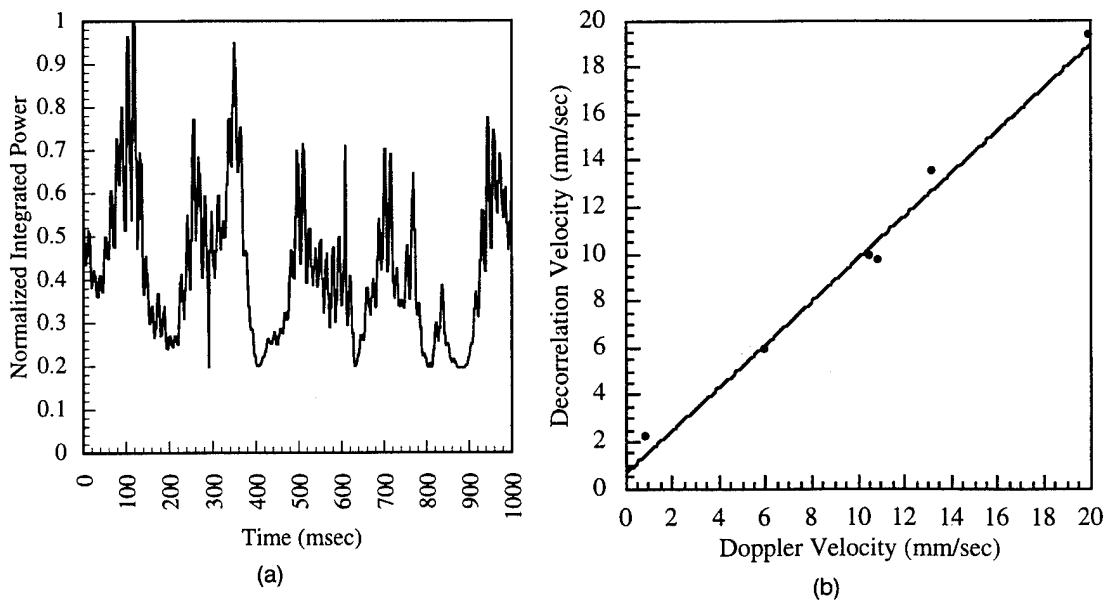

Fig. 2. Decorrelation results using spectral Doppler data. (a) The integrated power spectra at each time point. Note the appearance of a periodicity associated with the movement of speckle. (b) A comparison of the velocity calculated by the decorrelation and the standard Doppler shift technique. The line (slope = 0.91, $R^2 = 0.98$) is a linear fit of the data points.

sample volume when there is no net flow. This situation can occur in this case due to the large vessel diameter. It is expected that flow in small vessels (arterioles, venules, and capillaries, if Doppler shift is detected) will be more deterministic due to the greater physical constraints on the blood motion in the smaller vessels.

DISCUSSION

Because of the ubiquitous relationship of perfusion abnormalities to disease states and their therapies, a simple and accurate in vivo measurement of perfusion is highly desirable. Techniques that measure perfusion employ computed tomography (CT), magnetic resonance imaging (MRI) and nuclear medicine; these typically analyze kinetic profiles of contrast agents to extract tissue blood flow parameters (Beaney et al. 1984; Huang et al. 1982; Kallinowski et al. 1989; Miles 1991; Miles et al. 1993; Peters et al. 1987; Rosen et al. 1990). Beside the obvious need to inject contrast agents, these agents usually are not confined to the blood stream. Hence, difficulties arise in extracting true tissue blood flow from other parameters such as leakage of the agents into the soft tissue compartment. Some of this complexity can be removed with appropriate kinetic modeling (Adler 1987), but it seems doubtful that all of the multiple variables involved can be accounted for.

Ultrasound has some very attractive features for perfusion measurements. Since red blood cells, an inherently intravascular nondiffusible substance, are the primary source of ultrasound backscatter in blood, only perfusion is effectively being measured. Second, since most ultrasound contrast agents are microbubble based, they not only improve signal-to-noise ratio but are nondiffusible as well, unlike typical x-ray or magnetic resonance contrast agents. These ultrasound agents have already provided clinically useful information for perfusion of such tissues as the myocardium (c.f. Armstrong 1986; Kaul 1990; Wilson et al. 1993). Third, the nonlinear oscillation of bubbles makes it possible to separate flow signal from background signals even further by imaging the second harmonic of the transmitted ultrasound frequency (Shrope and Newhouse 1993). The bubble response at the second harmonic is proportionately much greater than the relatively weak response of static tissues. This tends to amplify flow signals relative to soft tissue making perfusion measurements much more practicable.

Dymling et al. (1991) used the first moment of the Doppler power spectrum for calculating perfusion. The method employs CW Doppler and has shown promise, working in a phantom and in a volunteer's finger. The method is somewhat geometry dependent,

and relies on an isotropic distribution of flows for an accurate estimate of perfusion; however, the promise of a contrast-free perfusion measure is intriguing.

Power Doppler imaging is a new ultrasonic technique for displaying blood flow with significantly improved sensitivity relative to conventional color Doppler imaging. It is essentially angle independent, and it is not subject to aliasing artifacts. Vessel morphology is well depicted using this technique, and the microvascular bed in some tissues has been shown to appear as a blush. This technique has shown considerable promise in mapping areas of perfusion, or its absence, in a number of clinical situations (Rubin 1993, in press). Detailed clinical studies are currently underway to better define its role (Newman et al. 1994). The major drawbacks of the technique in its current form relate to motion sensitivity and loss of velocity-related information. Further, in its current state, a parameter related to local blood volume rather than the actual blood flow is being encoded.

Atkinson and Berry (1974) have shown that the fluctuations of ultrasound pressure amplitude or fluctuations in the envelope derived from the pressure amplitude can generate information about motion through the beam. Approaching the problem from a purely statistical-based scattering theory in contrast to the dynamic approach we employed, they used a time domain cross-correlation technique to derive "fading" times that are similar to the decorrelation times we calculate from the power in the frequency domain (Doppler) signals. In fact, their Fig. 1b looks remarkably similar to our Fig. 2a. This is of further interest, since their "fading time" is based on motion transverse to the sound beam, whereas our spectra were obtained at 68°, thus containing both transverse and longitudinal speckle components. Since the properties of speckle are different across the beam as opposed to along the beam (Burkhardt 1978), we are encouraged that, at least in this single intermediate case, the results were somewhat immune to speckle morphology. Of course, our experiment 1, which employed color power imaging, only measured motion parallel to sound beam by design.

Also approaching this problem using statistical scattering theory arguments, Mo and Cobbold (1992) have suggested that the fluctuations in the amplitude of the Doppler signal relate to the rate at which scatterers move through a sampling region. This is manifested as a decorrelation time analogous to ours. It is interesting that similar conclusions can be drawn regarding dynamical behavior of the power in the Doppler signal whether starting from a scattering theory approach or using purely kinetic arguments such as ours.

The techniques using fluctuations in the Doppler

power have some definite advantages over the A-mode methods. The Doppler methods can be easily implemented, since the Doppler power spectrum is already calculated during standard spectral analysis, and the integration of these values to obtain the total power would be trivial. Second, the Doppler spectrum is already clutter canceled, removing soft-tissue motion, a significant source of noise. In fact, effective clutter cancellation already employed in obtaining the Doppler signal may be one of the biggest advantages in using the Doppler method, since the overwhelming signal from stationary tissue could confound any of these decorrelation techniques. While approached from different starting points, the two methods exhibit similarities, and A-line decorrelation techniques have already been used with success to image blood flow (Bamber et al. 1988).

We have demonstrated, in two simple flow phantoms, that the technique may allow one to measure local tissue perfusion using a correlation-based estimate of mean transit time. In fact, the mean velocity calculated from the normalized first moment of the Doppler power spectrum has a one-to-one correspondence (slope = 0.91, R^2 = 0.98, Fig. 2b) with the velocity calculated from mean transit time estimated from the decorrelation profiles and the known sample volume size over a broad range of flows employed in the second experiment. A critical feature in obtaining these estimates relates to sampling rate; undersampling can result in a situation analogous to aliasing in conventional Doppler, producing confusing decorrelation spectra. This is not surprising given the quasiperiodic nature of the raw power data (Fig. 2a). Alternatively, at sufficiently slow flow rates (expected in true capillary flow situations), simple exponential profiles were obtained, which resulted in unambiguous estimates of mean transit time.

A major assertion in this analysis is the validity of eqn (1), which requires that there be no other time scale comparable to the mean transit time through the region of interest. Second, the nature of the measurements being made are assumed to represent a stationary process, which seems to be a reasonable assumption (Mo and Cobbold 1992). Finally, we have assumed constant flow both locally as well as temporally. It is expected that the theory, as stated, can be generalized to more complex temporal flow dependencies. Further it is expected that in most situations a region of relatively constant flow can be selected so that one may avoid polydispersity in the distribution of flows for a given region.

This point may be moot, however, since the fluctuations in power that we are detecting are almost certainly not due to individual red blood cells but are caused by changes in coherent scattering, speckle, as groups of scatterers move through the sound beam. The effect of speckle moving in and out of the Doppler sample volume has produced a quasiperiodic spectrum even though the flow itself is constant (Fig. 2a). This fact alone may ultimately necessitate a more complex theoretical model beyond the simple exponential decorrelation demonstrated herein, even for constant flows. The entire process would be further complicated by the presence of turbulence, where multiple local velocities will cause rapid fluctuations in power due changes in scatterer density or coherent interference (Angelsen 1980; Shung et al. 1992; Twersky 1978). These changes would not reflect actual flow, although one could envision using such rapid, unexpected decorrelations as a measure of turbulence. Such circumstances would be highly unlikely in the slow flow, small vessel situations that we are interested in investigating, however. Nevertheless even with these potential problems, we have shown that the two-time power-derived correlation within a region-of-interest can be used to estimate mean flow. We currently plan to perform experiments in more physiologic flow phantoms (e.g., excised kidneys, etc.) in which quantitative estimates of perfusion in randomly configured vascular beds can be performed.

We have shown that the fluctuations inherent in deriving an estimate of mean scatterer number, and the basic multiframe nature of ultrasonic imaging, provides a simple scheme to estimate local tissue perfusion. The time scales over which fluctuations in mean scatterer number decorrelate may be regarded as mean transit time for passage of RBCs through the tissue volume of interest. We have shown this number to be a direct measure of specific flow. Having obtained this information, a true perfusion map may be derived.

REFERENCES

Adler, R. S. Generalized conservation equation for multicompartmental systems. Med. Phys. 14:218–222; 1987.

Angelsen, B. A. J. A theoretical study of the scattering of ultrasound from blood. IEEE Trans. Biomed. Eng. BME-27:61–67; 1980.

Armstrong, W. F. Assessment of myocardial perfusion with contrast enhanced echocardiography. Echocardiography 3:335–370; 1986.

Atkinson, P.; Berry, M. V. Random noise in ultrasonic echoes diffracted by blood. J. Phys. A: Math. Nucl. Gen. 7:1293–1302; 1974.

Bamber, J.; Hasan, P.; Cook-Martin, G.; Bush, N. Parametric imaging of tissue shear and flow using B-scan decorrelation rate. J. Ultrasound Med. 7:S135; 1988.

Beaney, R. P.; Lammertsma, A. A.; Jones, T.; McKenzie, C. G.; Halnan, K. E. Positron emission tomography for in vivo measure-

Determination of scan plane motion using speckle de-correlation. Part I. theoretical considerations and initial testing

Jian-Feng Chen, J. Brian Fowlkes, Paul L. Carson, and Jonathan M. Rubin

Department of Radiology
University of Michigan Medical Center
Ann Arbor, MI 48109

Abstract

In this paper, the correlation function of the echo signal intensities, which is directly related to the changes of speckle pattern on a series of B-mode images, is used to determine the scan-plane positions, motions, and orientations. It is assumed that the statistical properties of the echo signals follow those of a complex, circular Gaussian and the case is considered of diffusely scattering tissue with many fine particles per resolution cell and with no phase distortion. The random processes involved in forming these echo signals give rising to an uncertainty in the estimate this correlation function. This statistical uncertainty is analyzed using error propagation. Finally, the method is applied to 1-D array transducer, and initial results are presented from a tissue-mimicking phantom. Experimental results are in reasonable good agreement with the predictions. The method described in this paper can be applied to a clinical set when tissue can be modeled as a gelatin matrix containing many small randomly distributed point-like scatterers with uniform acoustic properties. The current method should serve as a baseline for the motion detection in general clinical applications.

INTRODUCTION

The purpose of this paper is to study the scan-plane motions through tissue and the estimate of their relative positions by analysis of speckle correlation in ultrasonic images. Conventionally, the second-order statistics were used to study the correlation of speckle patterns at different locations within ultrasonic images for tracking the relative motion of blood or other moving tissue [1]. Speckle correlation has also been studied for the purpose of the speckle reduction for improving lesion detectability via spatial and frequency compounding [2, 3, 4, and 5]. These speckle reduction methods involve the averaging of images in which the speckle pattern has been changed. In this paper we will use the speckle correlation between corresponding points in a series of scan-planes for an alternative purpose: to determine the relative scan-plane positions, motions, and orientations. This may be important for the 3-D registration of ultrasonic images, or the detection and correction for tissue motion.

Speckles on conventional B-mode images are caused by the phase-sensitive detection of the scattering from random inhomogeneities in the acoustic properties of biological tissue in the resolution cell of the transducer. When the scan-plane is moved slowly, the intensities of time domain echo signals at one distance along one echo line change, producing a change in the speckle patterns observed at that location on the B-mode images. We will analyze the second-order statistical properties of the echo signal intensity at a given depth as a function of time or image frame number, instead of tracking the speckle patterns in subsequent images as a function of position within the images. The second-order statistics are defined as the expectation of the product by pairs of values (intensities) measured at two positions in space, number of frame or time.

In this paper, it is assumed that the statistical properties of echo signals follow those of a complex, circular Gaussian and the case is considered of diffusely scattering tissue with many fine particles per resolution cell [2] and with no phase distortion [6]. The method, in which the correlation function of echo signal intensities are used to determine the relative positions of scan planes and their motions, is proposed. Then, the statistical uncertainty of this correlation function estimate is analyzed using error propagation. Finally, the method is applied to 1-D array transducer and the initial results are presented from testing a tissue-mimicking phantom.

I. THEORY

a. The correlation of speckle pattern in B-mode images

The speckles in B-mode images are directly related to the echo signal intensities or their magnitudes. The correlation function of the intensities for a purely random (diffusely scattering) case can be estimated from the correlation function of the complex echo signals. The correlation of the echo signal intensities between two specific positions separated by $\Delta \vec{r}$, e.g., $\vec{r}$ and $\vec{r} + \Delta \vec{r}$, is defined as

$$R(\Delta \vec{r}) = <I(\vec{r})I(\vec{r} + \Delta \vec{r})> \tag{1}$$

where $I(\vec{r}) \equiv |U(\vec{r})|^2$ and $I(\vec{r} + \Delta \vec{r}) \equiv |U(\vec{r} + \Delta \vec{r})|^2$ are the intensities of the echo signals at specific two points $\vec{r}$ and $\vec{r} + \Delta \vec{r}$. $U(\vec{r})$ and $U(\vec{r} + \Delta \vec{r})$ are the complex echo signals. $<...>$ stands for the expectation of a random variable.

Using the moment theorem for the jointly normal, zero mean, Gaussian random

variables, and assuming that the real and imaginary parts of the complex echo signal $U(\vec{r})$, $U_r(\vec{r})$ and $U_i(\vec{r})$, are uncorrelated, *e.g.*

$$\langle U_r(\vec{r})U_i(\vec{r}+\Delta\vec{r})\rangle = \langle U_r(\vec{r}+\Delta\vec{r})U_i(\vec{r})\rangle = 0,$$

we have [7]

$$R(\Delta\vec{r}) = 2\langle U_r^2(\vec{r})\rangle\langle U_r^2(\vec{r}+\Delta\vec{r})\rangle + 4\langle U_r(\vec{r})U_r(\vec{r}+\Delta\vec{r})\rangle^2 + 2\langle U_i^2(\vec{r})\rangle\langle U_i^2(\vec{r}+\Delta\vec{r})\rangle.$$

Using the symmetry of the correlation function of the complex echo signals $U(\vec{r})$,

$$\rho(\Delta\vec{r}) = \frac{\langle U(\vec{r})U^*(\vec{r}+\Delta\vec{r})\rangle}{<I>}, \tag{2}$$

Finally, we have

$$R(\Delta\vec{r}) =<I>^2 (1+\|\rho(\Delta\vec{r})\|^2) \tag{3}$$

or

$$\|\rho(\Delta\vec{r})\|^2 = \frac{R(\Delta\vec{r})}{<I>^2} - 1 \tag{3'}$$

where $<I>$ is the average echo signal intensity over the region of interest. Here $\|\rho(\Delta\vec{r})\|^2$ is called the normalized correlation of the echo signal intensities and is denoted by $\Gamma(\Delta\vec{r})$.

Equations (3) and ($3'$) show that there is a simple relationship between the correlation function of the complex echo signals and the correlation function of the signal intensities, which is directly related to the speckle on B-mode images.

b. Applying for clinical scanners

The ideal instruments for the 3-D ultrasonic imaging currently are array scanners, here a 1-D linear array will be considered. To further simplify our analysis, we confine our measurements in the focal zone or Fraunhofer region of the array transducer. Applying the Huygens-Freanel principle, the radiating surface of the transducer as a collection of point sources that oscillate sinusoidally is considered. If the sources lie entirely within a simple plane (x',y') as shown in Figure 1, the radiating surface is defined by an aperture distribution function [8]

$$a(x',y') = \frac{1}{DWh/d}\left\{\left[rect\left(\frac{x'}{D}\right)\frac{1}{b}comb\left(\frac{x'}{d}\right)\right]\otimes\left[rect\left(\frac{x'}{d}\right)\right]\right\}rect\left(\frac{y'}{h}\right) \tag{4}$$

where (x',y') is a point on the transducer surface. W is the width of array elements, d is the center-to-center distance between array elements, D is the array transducer dimension, h is the height of array elements in the elevation direction, and functions

$$comb(x) = \sum_{i=-\infty}^{+\infty}\delta(x-i)$$

Page 4

and

$$rect(x) = \begin{cases} 0 & |x| > 1/2 \\ 1 & |x| \le 1/2 \end{cases}.$$

When the pulsed transducer is used to insonify a medium containing randomly distributed fine particles, the complex echo signal is given by [8]

$$U(\vec{r}) \sim C \frac{e^{2ikz}}{z^2} h_1^2(x,y) \tag{5}$$

where $k = 2\pi / \lambda_o$ is the ultrasound wave number, λ_o is ultrasound wave length at its central frequency, z is a distance along beam axis from the surface of the transducer to the field point, and $h_1(x,y)$ is called the directivity function and is specified entirely in the (x,y) plane (within the region of the interest) when the assumption of local plane-wave exists. For a 1-D array transducer, the directivity function is given by [8]

$$h_1(x,y) \approx \left[\sum_{i=-\infty}^{+\infty} \sin c(\frac{wx}{\lambda_o z}) \sin c(\frac{Dx}{\lambda_o z} - \frac{iD}{d}) \right] \sin c(\frac{hy}{\lambda_o z}) . \tag{6}$$

where .
Here the motion of scan-plane in the perpendicular direction related to scan plane (called the elevation direction) is considered. In that case, the normalized correlation function of the echo signal intensities will depend just on the properties of transducer in that direction and is given by

$$\Gamma(\Delta y_i) \approx (\sin c^2 y_o \otimes \sin c^2 y_o)^2 \tag{7}$$

where $\otimes$ stands for a convolution operator. $\Delta y_i = i \times \delta y$ is a displacement in the elevational direction, i is the number of step, and δy is the step size. $y_o = (h\Delta y_i)/(\lambda_o z)$. Equation (7) shows that the correlation function, $\rho(\Delta y)$, depends on the parameter y_o and echo signals will be completely de-correlated when $y_o \ge 2$. As shown in Figure 2, the function given by Equation (7) could be well approximately insteaded by a Gaussian function

$$\Gamma(\Delta y_i) \approx e^{-2a_o(\Delta y_i)^2} \tag{7'}$$

where $a_o \approx 2.72h^2 / (\lambda_o z)^2$.

II.   EXPERIMENTAL PROCEDURES AND RESULTS

Experiments were performed to test the proposed method to determine the relative positions of scan planes by using the correlation of speckles in B-mode images. A 3.5 MHz array transducer, with an 6 mm of the elevational length and a 3.5 cm of the radius of curvature, was directly used to collect imaging data within the region of the interest in a tissue-mimicking phantom, which contains randomly distributed point-like particles. In order to determine the

accurate correlation function, the step size is set as $\delta y = 0.1$ *mm* in our experiment.

At first, for each point within the region of interest, the pixel value is converted to a linear scale by $I(\vec{r}) \approx 10^{P(\vec{r})/P_o}$, where $P(\vec{r})$ is raw B-mode imaging dB data, and the constant P_o is used to convert from a 0-255 log scale for intensity to a linear scale. Then, the experimental result of the normalized correlation function of the echo signal intensities among different image frames is determined by

$$\Gamma(\Delta y_i) \approx \frac{(m \times n) \sum_{j=1}^{m} \sum_{k=1}^{n} I_{j,k}(\vec{r}) I_{j,k}(\vec{r} + \Delta y_i \vec{e}_y)}{\left\{ \sum_{j=1}^{m} \sum_{k=1}^{n} I_{j,k}(\vec{r}) \right\}^2} - 1, \tag{8}$$

here the average is over the region of interest, *e.g.* $m \times n$ pixels. Then, the correlation function of echo signal intensities can be determined by using Equation (8). Finally, a Gaussian curve is used to fit the experimental results, and the step size, δy, can be estimated based on the coefficient in that fitting curve.

In order to examine the effect of this slice positioning technique on a 3-D image reconstruction and to further indicate its accuracy, images of a tissue mimicking phantom from the 3.5 MHz array transducer were made using a mechanical positioning system. The system was specifically designed for breast scans, but has also been successfully used to scan a transplanted kidney and some tissue mimicking phantoms [9]. The images were then processed to determine the image-based spacing that would have been calculated. Post-processing of images was implemented in a modular code under a AVS (Advanced Visual Systems, Inc. Waltham, MA) and run on a Sun Sparcstation. Images were collected from an ultrasound scanner and read into the workstation memory. The RGB images are then processed to select one channel for B-mode and then the 3-D data set is sliced and a single 2-D plane displayed to select regions of interest (ROI) to be processed for determining the slice separation. The pixels contained in the ROI in each image are converted to a 1-D vector and the process repeated for each image. Each of these vectors are then combined in a 2-D vector. The group of image ROIs, which are at the same depth on B-mode images, are then analyzed to compute the correlation between successive ROIs, *i.e.* ROI#1 correlation to ROI#2, ROI#2 to ROI#3, etc. for a one step correlation values. Then the process is repeated for two, three, etc step correlation. For this test, ROIs from groups of ten images were used to determine the slice separation for the center two slices, *e.g.*, to position image 6 with respect to 5 use information from images 0-9, for image 7 after 6 use image 1-10, *etc*. This does assume a piece-wide smooth motion for the scan-head but this is considered a reasonable first approach to the position estimate. In each case, the correlation curve was fit using a least squares approach to the Gaussian function as shown in Equation (7'). This information is then used to position the images on an arbitrary grid space and correctly positioned images can then be displayed.

A typical measurement result of the correlation function of the echo intensities as well as its Gaussian fitting curve are shown in Figure 3. Based on this Gaussian fitting curve, the optimal value of the step size can be determined at that specific depth. Similarly, a group of the correlation functions are given in Figure 4 when the scan-head mechanically moved through the phantom in elevational direction. Then, the space between image planes is determined based on the coefficients of these correlation functions. The average calculated image spacing was (0.17 ± 0.01) mm where the predict value was 0.17 mm. The mean and standard deviation of the step size are calculated based on several regions of interest at the depth. This indicates that

the estimating technique is working quite well.

III. DISCUSSIONS

As shown in the current paper, the results of correlation between successive images can indicate the distance traveled accurately. There are a number of ways to use this information to monitor scanner motion. Many of these can be thought of simply by reversing the concepts currently used to measure tissue motion. The following are a few example implementations for monitoring scanner motion using this correlation techniques alone or in the combination with other methods of motion detection.

1. Monitoring tilt and rotation of transducer.

Measuring different motions at different locations within images will indicate the transducer motion which is not uniform in the elevational direction. For example, tilting the transducer slightly can be detected by examining the de-correlation at different depths in the image as long as the depth dependent *psf* (point spread function) is well defined. In addition to tilt angle, transducer rotation might be tracked. For example, several different ROIs corrected for the *psf* in these regions, could be monitored such that differences among these regions provide relative motion information. The difference in rate among these images would indicate tilting of the scan-head. This measurement could be performed across the entire outlined region comparing the value in the region proximal to the transducer to that of the corresponding distal value of the same lateral location.

2. On-the-fly processing of position information.

By restricting the regions which are measured for motion, it may be possible to minimize the computational time to the point where such monitoring can be performed in real-time. The advantage would be that the position information could be computed at a rate faster than the frame rate of the imaging system. Also it may be possible to set motion criteria which will indicate when the images should be taken to provide an automated way of reducing the number of frames acquired in the 3-D data set and fix their spacing to make reconstruction simpler.

3. Correction for tissue motion such as respiratory motion.

These speckle de-correlation techniques could also allow for the correction of respiratory motion when 3-D data set are reconstructed. Elevational as well as in plane correction to keep a region of interest stationary in the image.

4. Detection of phase aberrations.

The rate that the speckle pattern is changing can also indicate the presence of phase aberrators in the field of view for the scan-head. By looking at various regions of the image, sudden or inconsistent regional changes in correlation rates will indicate an aberration of phase. Such mapping could predict which data to throw out of some images when compounding or reconstructing in 3-D or perhaps when and where phase aberration correction would need to be performed in the images.

5. Use of technique with current coarse positioning.

The currently described technique could also be used for fine positioning in conjunction with other positioning systems. The latter could monitor the long range motion of the scan-head but lack the fine spatial resolution required for the best 3-D reconstructions. Such encoding devices include optical, mechanical, magnetic, electric spark systems, *etc*. All of which have been used in the past for 3-D ultrasound imaging.

7. Combination of 2-D speckle tracking and de-correlation.

One possible implementation would incorporate 2-D speckle tracking [1] to monitor motion in the scan plane between adjacent slices and then measure the de-correlation result. The idea is that the 2-D speckle tracking would identify the correct vertical and horizontal translation

required for placing the adjacent slice with respect to the first. The de-correlation which then remained between the slices would be the result of the translation in the elevational direction and would be an improved estimate over assuming no vertical or horizontal motion.

IV. CONCLUSIONS

In this paper, a method using the correlation of echo signal intensities in B-mode images, which is directly related to the changes of speckle pattern, in the elevation direction for determining the scan-plane relative positions and their motions is described. The method was tested using a tissue mimicking phantom containing randomly positioned fine solid particles. The experimental result was in reasonable good agreement with the prediction. However, the current method for the de-correlation of the speckle can only be applied to a clinical set when tissue can be modeled as a gelatin matrix containing many small randomly distributed point-like scatterers with uniform acoustic properties. Nevertheless, the current method should serve as a baseline for the motion detection based on the correlation of speckles.

ACKNOWLEDGMENTS

APPENDIX

We consider a complex random process, *e.g.* the complex echo signal, including both an amplitude and a phase information. We are interested in the correlation function of the complex echo signals between two subsequent scan plane positions. The complex echo signals are given by [8]

$$U(\vec{r}) = U_r(\vec{r}) + iU_i(\vec{r})$$

and

$$U(\vec{r} + \Delta\vec{r}) = U_r(\vec{r} + \Delta\vec{r}) + iU_i(\vec{r} + \Delta\vec{r})$$

where $\vec{r}$ and $\vec{r} + \Delta\vec{r}$ are the positions within a region of interest related to the transducer scan head. The completely random signals are taken to have zero mean and to have the same variances of the real and imaginary parts. Then the auto-correlation function of the resulting signal is given by

$$\rho(\Delta\vec{r}) = < U(\vec{r})U^*(\vec{r} + \Delta\vec{r}) > \tag{A-1}$$

where * refers to the complex conjugation, and displacement between points in the two scan planes is given by $\Delta\vec{r}$. If this field is simply read out or scanned by an imaging system with a point-spread function (*psf*) $h(\vec{r})$, the resulting complex signal $U(\vec{r})$ is related to the original field $\alpha(\vec{r})$ by

$$U(\vec{r}) = h(\vec{r}) \otimes \alpha(\vec{r}) \tag{A-2}$$

where $\otimes$ is a convolution operation and $\alpha(\vec{r})$ depends on the properties of the medium. The correlation function of the resulting processing, $\rho(\Delta\vec{r})$ is then directly given by [7]

$$\rho(\Delta\vec{r}) = h(-\Delta\vec{r}) \otimes \rho_\alpha(\Delta\vec{r}) \otimes h^*(\Delta\vec{r}) \tag{A-3}$$

where $\rho_\alpha(\Delta\vec{r}) \equiv < \alpha(\vec{r})\alpha^*(\vec{r} + \Delta\vec{r}) >$. Equation (A-3) shows that the correlation function depends on the displacement of the beam related to scatterers in the region of interest.

A typical example is the acoustic scattering from a random collection of N scatterers in and extending well beyond a resolution cell or volume. These N scatterers can be divided into L sets, each set containing N_l scatterers ($\sum_{l=1}^{L} N_l = N$), and all having the same displacement, $\Delta\vec{r}_l$ from the previous set. In that case, we have

$$\alpha(\vec{r}) = \sum_{i=1}^{N} |a_i| e^{i\phi_i} \tag{A-4}$$

and

$$\alpha(\vec{r} + \Delta\vec{r}) = \sum_{j=1}^{N} |a_j| e^{i\phi_j} \tag{A-5}$$

where a_i is the magnitude of the scattering amplitude of the i th scatterer and there is correlation neither among the scatter phase ϕ_i in the first scattering volume nor among those in the second scattering volume nor between the scattering volumes. Then the correlation function of $\alpha(\vec{r})$ is

$$< \alpha(\vec{r})\alpha^*(\vec{r} + \Delta\vec{r}) > = \sum_{i=1}^{N}\sum_{j=1}^{N} <|a_i||a_j| e^{i(\phi_i - \phi_j)}$$

$$= \sum_{l=1}^{L}\left\{ N_l |a_l|^2 \delta(\Delta\vec{r}_l) \right\}, \tag{A-6}$$

since all phases average out unless they match up identically. Here $\delta(\Delta\vec{r}_l)$ is the Dirac delta function.

Finally, the correlation function of the readout or scanned process is then simplified to

$$\rho(\Delta\vec{r}) = \sum_{l=1}^{L} \rho_l(\Delta\vec{r}_l) \tag{A-7}$$

where $\rho_l(\Delta\vec{r}_l)$ is given by

$$\rho_l(\Delta\vec{r}_l) = N_l \|a_l\|^2 \left\{ h(-\Delta\vec{r}_l) \otimes h^*(\Delta\vec{r}_l) \right\} . \tag{A-8}$$

In the far field or the focal zone of the transducer, the *psf* can be approximately separated into the transverse component due to the diffraction limited beam, and the axial component due to the ultrasonic pulse

$$h(\Delta\vec{r}) \approx h_t(r_t)h_r(r_r) \tag{A-9}$$

where $h_t(r_t)$ and r_t are the transverse components of the *psf* and the displacement of the scatterers, and $h_r(r_r)$ and r_r are the axial components of the *psf* and the displacement of scatterers. As a simple example, when all scatterers are in motion (relative to the scan head) in the lateral direction, the correlation function of the complex echo signal will just depend on the transducer beam properties when the scatterers are in motion in the axial direction, that function will depend on the ultrasonic pulses.

REFERENCE

1. E.J. Chen, W.K. Jenkins, and W.D. O'Brien. Jr, "The accuracy of precision of estimating tissue displacements from ultrasonic image," IEEE Trans. Sonics Ultrason. Symposium (1992).

2. R.F. Wagner, S.W. Smith, J.M. Sandrik, and H. Lopez, "Statistics of speckle in ultrasound B-scans," IEEE Trans. Sonics Ultrason., vol. SU-30, pp 156-163 (1983).

3. S.W. Smith, R.F. Wagner, J.M. Sandrik, and H. Lopez, "Low contrast detectability and contrast/detail analysis in medical ultrasound," IEEE Trans. Sonics Ultrason., vol. SU-30, pp 164-173 (1983).

4. G.E. Trahey, S.W. Smith, and O.T. Von Ramm, "Speckle pattern correlation with lateral aperture translation: experimental results and implications for spatial compounding," IEEE Tran. Sonics Ultrason., vol. SU-33, pp 257-264 (1996).

5. M. O'Donnell, and S.D. Silverstein, "Optimum displacement for compound image generation in medical ultrasound," IEEE Trans. Sonics Ultrason., vol. SU-35, pp 470-476 (1983).

6. L. Nock, G.E. Trahey, "Phase aberration correction in medical ultrasound using speckle brightness as a quality factor," J. Acoust. Soc. Am., 85, pp 1819-1833 (1989).

7. R.F. Wagner, M.F. Insana, and D.G. Brown, "Statistical properties of radio-frequency and envelope-detected signals with applications to medical ultrasound," J. Opt.. Soc. Am.A. Vol. 4, pp 910-922 (1987).

8. M.F. Insana, T.J. Hall, and L.T. Cook, "Backscatter coefficient estimation using array transducers," IEEE Trans. Sonics Ultrason., vol. SU-41, pp 714-723 (1994).

9. A. Moskalik, P.L. Carson, C.R. Meyer, J.B. Fowlkes, J.M. Rubin, M.A. Roubidoux, "Registration of 3D compound ultrasound scans of the breast for refraction and motion correction," Ultrasound in Med. and Biol., accepted (1994).
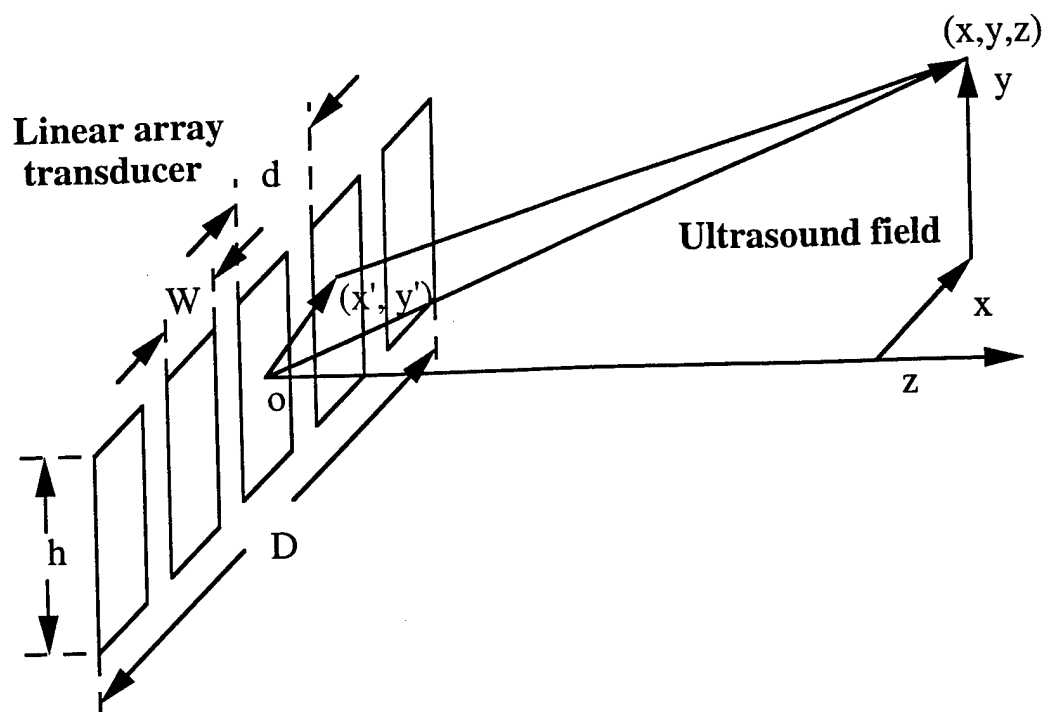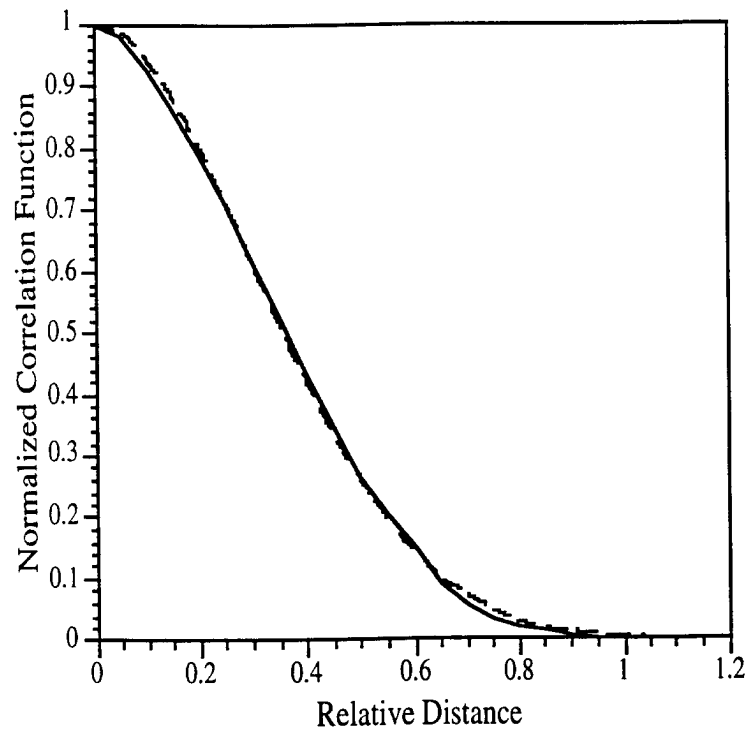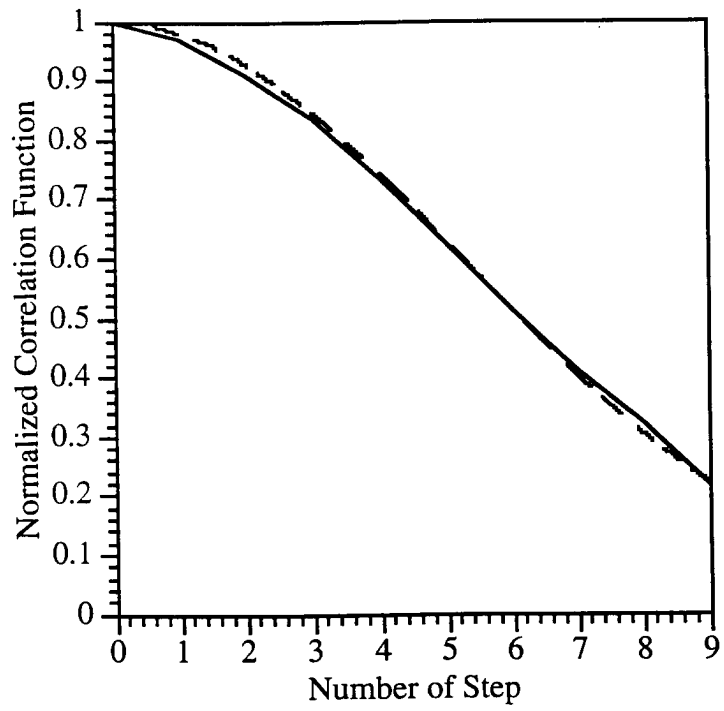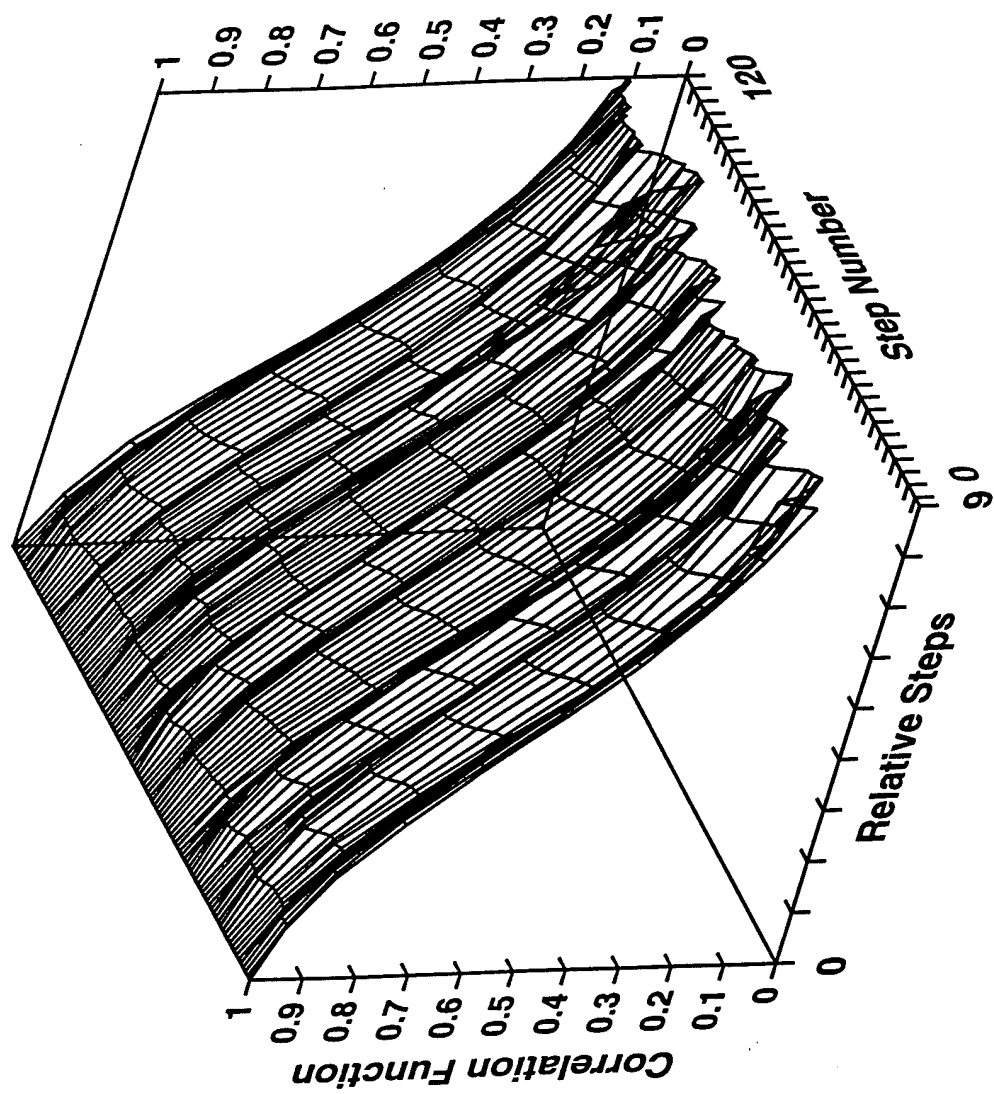
Figure 1

Figure 2

Figure 3

Figure 4

ABSTRACT

In a previous paper [1], a method for determining the scan-plane positions, motions, and orientations is proposed based on the de-correlation of speckle on a series of B-mode images. This method involves evaluating the second-order statistics of echo signal intensities among the images slices within regions of interest. The random processes involved in forming these echo signals give rise to an uncertainty in the estimate this auto-correlation function. This statistical uncertainty is evaluated here using the error propagation. The statistical uncertainty depends on the effective number of independent speckle spots in a 3-D region of the interest used to estimate this auto-correlation function. Further experiments are reported in the current paper.

INTRODUCTION

In a previous paper [1], we studied a method to estimate scan plane motions and their relative positions by using the de-correlation of the speckles in ultrasonic B-mode images. Initial results show that the method could be used to determine the relative positions effectively. The purpose of this paper is more detail to study the experimental condition which is required to get more accurate results, and to show more experimental results.

As given in the previous paper, in this paper it is assumed that the statistical properties of echo signals follow those of a complex, circular Gaussian and the case is considered of diffusely scattering tissue with many fine particles per resolution cell [2] and with no phase distortion [3]. The method involves evaluating the second-order statistics of echo signals. The random processes involved in forming these echo signals give rise an uncertainty in the estimate the second-order statistics. This statistical uncertainty is evaluated here first using error propagation.

I. THEORY

a. Statistical uncertainty of the correlation function of speckles in B-mode images

The correlation of the echo signal intensities, which is related to the de-correlation of speckles between two specific positions, e.g. $\vec{r}$ and $\vec{r} + \Delta\vec{r}$ is given by

$$R(\Delta\vec{r}) = < I(\vec{r})I(\vec{r} + \Delta\vec{r}) > \tag{1}$$

where $I(\vec{r})$ and $I(\vec{r} + \Delta\vec{r})$ are the echo signal intensities at these two positions. $\Delta\vec{r}$ is the displacement between two points in the region of interest. Thus, the relative scan plane positions and their motions can be determined from this correlation function [1].

To compute the auto-correlation function of the imaging intensity effectively, we must determine how big of a region of interest is needed to determine this correlation function within a specific statistical uncertainty. This includes two things: 1) the relationship between the independent number of samples and statistical uncertainty of the auto-correlation function; 2) the relationship between the number of independent sample and a volume of region of interest.

In our experiment, we use the following equation to determine the correlation function of echo signal intensities

$$\Gamma(\Delta\vec{r}) \approx \frac{J_1}{J_2^2} - 1 \tag{2}$$

where $J_1 \equiv << I(\vec{r})I(\vec{r} + \Delta\vec{r}) >>$, $J_2 \equiv << I(\vec{r}) >> \approx << I(\vec{r} + \Delta\vec{r}) >>$, and $<<...>>$ stands for the experimental sample means of random variables $I(\vec{r})I(\vec{r} + \Delta\vec{r})$ and $I(\vec{r})$. The variance of the variable $R(\Delta\vec{r})$ is given by [4]

$$\sigma_\Gamma^2 = \left(\frac{\partial\Gamma}{\partial J_1}\right)^2 \sigma_{J_1}^2 + \left(\frac{\partial\Gamma}{\partial J_2}\right)^2 \sigma_{J_2}^2 + 2\left(\frac{\partial\Gamma}{\partial J_1}\right)\left(\frac{\partial\Gamma}{\partial J_2}\right)\sigma_{J_1 J_2}^2$$

$$\approx \frac{1}{J_2^4}\sigma_{J_1}^2 + 4\frac{\Gamma^2}{J_2^2}\sigma_{J_2}^2 - 4\frac{\Gamma}{J_2^3}\sigma_{J_1 J_2}^2 \tag{3}$$

where

$$\sigma_{J_1}^2 = \frac{1}{M}(< I^2(\vec{r})I^2(\vec{r} + \Delta\vec{r}) > - < I(\vec{r})I(\vec{r} + \Delta\vec{r}) >^2)$$

$$= \frac{1}{M}(4k_1 - \Gamma^2) <I>^4,$$

$$\sigma_{J_2}^2 = \frac{1}{M}(<I^2(\vec{r})> - <I(\vec{r})>^2) = \frac{1}{M}<I>^2$$

and

$$\sigma_{J_1 J_2}^2 = \frac{1}{M}<\{[I(\vec{r})I(\vec{r}+\Delta\vec{r}) - <I(\vec{r})I(\vec{r}+\Delta\vec{r})>][I(\vec{r}) - <I(\vec{r})>]\}>$$

$$= \frac{1}{M}(2k_2 - \Gamma)<I>^3.$$

Here M is the number of independent of samples in the region of interest used to determine the sample mean of the random variables[5], and the constants k_1, k_2, and Γ could be determined by the relative positions of two points $\vec{r}$ and $\vec{r}+\Delta\vec{r}$. Using the complex Gaussian statistical properties of the echo signals, the values of these constants can be determined, and their values will be within $k_1 \in [1,6]$, $k_2 \in [1,3]$, and $\Gamma \in [1,2]$ [6]. Equation (A-2) is simplified to

$$\sigma_R^2 = \frac{1}{M}(4k_1 - 8k_2R + 7R^2) \tag{4}$$

As an example, we consider two limitation cases:

(a) When $\Delta\vec{r} = 0$, we have $k_1 = 6$, $k_2 = 3$, and $\Gamma = 2$. Therefore, $\sigma_\Gamma^2 = 4/M$;

(b) When $\Delta\vec{r} = \infty$, we have $k_1 = 1$, $k_2 = 1$, and $\Gamma = 1$. Therefore, $\sigma_\Gamma^2 = 3/M$.

In general case, we have $0 \le \Delta\vec{r} \le +\infty$. Therefore, the variance of the auto-correlation function is given by

$$\frac{3}{M} \le \sigma_\Gamma^2 \le \frac{4}{M}. \tag{5}$$

That means the variance of the auto-correlation function is directly related to the number of independent data samples M. Using the statistics of the image intensity, it is not difficult to determine the number of independent data samples M, which is related to the statistics of the sample mean of the image intensity as well as the variance of the intensities [7].

b. Error analysis in the fitting curve

In our measurement, Equation (7) in reference 1 is used to fit the experimental data ρ_{io} at different displacement $\Delta y_i = i \times y_c$ to determine the relative positions of the scan planes (called the step size), where i the number of the step and y_c is the step size. It is important to determine the uncertainties involved in this technique.

The difference between a Gaussian fitting curve and the experimental data is noted by

$$L(y_c) = \sum_{i=1}^{N}(\rho_i - \rho_{io})^2 \tag{6}$$

where N is the total number of steps, ρ_{io} is the measured values of the auto-correlation function at a different displacement Δy_i and $\rho_i = \rho(\Delta y_i)$.

The optimized step size, y_c, could be determined from the condition of the minimum $L(y_c)$. That is

$$F(y_c) \equiv \frac{1}{2} \times \frac{\partial L(y_c)}{\partial y_c}$$

Page 4

$$= \sum_{i=1}^{N} (\rho(\Delta y_i) - \rho_{io}) \frac{\partial \rho(\Delta y_i)}{\partial y_c} = 0 . \qquad (7)$$

As shown in the reference 1, a Gaussian function $\rho(\Delta y_i) \approx e^{-a_o(\Delta y_i)^2}$ is well approximated as the theoretical prediction of the de-correlation function, where $a_o = 2.72h^2 / (\lambda_o z)^2$. In that case, we have

$$F(y_c) = -2a_o y_c \sum_{i=1}^{N} \left[i^2 (e^{-a_o i^2 y_c^2} - \rho_{io}) e^{-a_o i^2 y_c^2} \right] = 0. \qquad (8)$$

If the measured values of the auto-correlation function at different displacements are independent, the uncertainty of the step size y_c will be given by

$$\delta^2 y_c = \sum_{j=1}^{N} \left[\left(\frac{\partial y_c}{\partial \rho_{jo}} \right)^2 \times \left(\delta \rho_{jo} \right)^2 \right] \qquad (9)$$

where $\delta \rho_{io}$ is the uncertainty of the measurement result of the auto-correlation function at step i, and

$$\frac{\partial y_c}{\partial \rho_{jo}} = - \frac{\left(\partial F / \partial \rho_{jo} \right)}{\left(\partial F / \partial y_c \right)}$$

$$= \frac{-y_c j^2 \rho_j}{\sum_{i=1}^{N} \left[2a_o i^4 y_c^2 \rho_i^2 + i^2 \rho_i (\rho_i - \rho_{io})(2a_o i^2 y_c^2 - 1) \right]}. \qquad (10)$$

If the uncertainties of the measured auto-correlation function for all steps are almost the same, $\delta \rho \approx \delta \rho_{j_o} \equiv \rho_i - \rho_{io}$, Equation (9) can be simplified to

$$\left(\frac{\delta y_c}{y_c} \right)^2 = \frac{\sum_{i=1}^{N} \left(i^4 \rho_i^2 \right)}{\left\{ \sum_{i=1}^{N} \left[2a_o i^4 y_c^2 \rho_i^2 + i^2 (2a_o i^2 y_c^2 - 1) \rho_i \delta \rho \right] \right\}^2} \delta^2 \rho. \qquad (11)$$

II.   EXPERIMENTAL PROCEDURES AND RESULTS

Experiments were performed to test the proposed method to determine the relative positions of scan planes by using the correlation of the speckles on B-mode images. A 5.0 MHz array transducer, with the elevation length is $h=6$ mm and the radius curvature for the transducer is $r=3.5$ cm, was directly used to collect imaging data within the region of the interest in a tissue-mimicking phantom, which contains randomly distributed point-like particles. When $\Delta r_i \geq 1.7mm$ the echo signal will be completely de-correlated, in order to determine the accurate correlation function, the step size is 0.1 mm in our experiment.

At first, for each point within the region of interest, the pixel value is then converted to a linear scale [7]

$$I(\vec{r}) \approx 10^{P(\vec{r})/P_o}$$

Page 5

where $P(\vec{r})$ is raw dB data, and the factor P_o is used to convert from a 0-255 log scale for intensity to a linear scale. Then, the correlation function of the echo intensities is given by

$$\Gamma(\Delta y_i) \approx \frac{(m \times n)\sum_{j=1}^{m}\sum_{k=1}^{n} I_{j,k}(\vec{r})I_{j,k}(\vec{r}+\Delta y_i \vec{e}_y)}{\left\{\sum_{j=1}^{m}\sum_{k=1}^{n} I_{j,k}(\vec{r})\right\}^2} - 1 , \tag{12}$$

Here the average is over the region of the interest, e.g. $m \times n$ pixels. Then Equation (7) of reference 1 is used to fit the experimental result and to find an optimal step size y_o.

A typical result of the auto-correlation functions based on Equations (12) and its Gausssian fitting curve based on Equation (7) in reference 1 is shown in Figure 1. From its fitting curve, the optimal value of the step size can be estimated. In order to further test this method, two experiments were performed by using a mechanical scanning system as well as hand scanning for imaging a contrast detail phantom. The images from a 3.5 MHz array transducer were then processed to determine the image-based spacing that would have been calculated. Post-processing of images was implemented in a modular code under a AVS (Advanced Visual Systems, Inc. Waltham, MA) and run on a Sun Sparcstation. Images were collected from an ultrasound scanner and read into the workstation memory. The RGB images are then processed to select one channel for B-mode and then the 3-D data set is sliced and a single 2-D plane displayed to select regions of interest (ROI) to be processed for determining the slice separation. The pixels contained in the ROI in each image are converted to a 1-D vector and the process repeated for each image. Each of these vectors are then combined in a 2-D vector. The group of image ROIs which are at the same depth on B-mode images are then analyzed to compute the correlation between successive ROIs, i.e. ROI#1 correlation to ROI#2, ROI#2 to ROI#3, etc. for a one step correlation values. Then the process is repeated for two, three, etc step correlation. For this test, ROIs from groups of ten images were used to determine the slice separation for the center two slices, e.g., to position image 6 with respect to 5 use information from images 0-9, for image 7 after 6 use image 1-10, etc. This does assume a piece-wide smooth motion for the scan-head but this is considered a reasonable first approach to the position estimate. The results of the correlation functions changed with step number, when the scanner was moved through the surface of the phantom, are shown in Figures 2 and 3. In Figure 2, it is not difficult to find the correlation functions are very stable when the step number is increased, because the uncertainty of the step size, which is determined by the accuracy of the mechanical scanning system, is very small (about 10 μs). Figure 3 shows the correlation functions changes with the step number when using hand scanning, since it is difficult to keep the same speed when the scanner moving through the surface the phantom by hand and the step size may be changed during the scanning. Then, the step size between image plane was estimated based on the Gaussian fitting curves for the correlation function in several regions of interest at the same depth. The result shows that the estimate error of the step size for hand scanning, which is about 15 %, or (0.175 ± 0.024) mm, is larger than that for the mechanical scanning, which is about 8 %. Finally the results of these two approach (using mechanical scanning as well as hand scanning) are shown in Figure 4, in which the high contrast cone is not significantly different when using either the known slice separation or that calculated using image information (speckle de-correlation). The first image is a longitudinal view of cone object from the curved array 3.5 MHz transducer based on hand scanning using equal step size, while the second image is the same view based on the hand scanning using the actual step size estimated by correlation of speckle, and the last on is a subtract image between the first and the second images (expanded horizontally). For the hand scanning, the images

Page 6

were recorded at 32 fps in a 120 frame cine loop. Results given in Figure 4 asow the appearance of the echogenic cone is not very different for this short scan when using either an equal slice separation assuming uniform hand scanning rate or that calculated using the image decorrelation rate. However, the lower graphs illustrate the decorrelation does track smoothly the non-uniform motion. Black stripes in the subtraction image correspond to zeros in the integral displacement error of the uniform stepping as plotted in the graph on the right. The results of these images indicate that the estimating technique is working quite well at this early stage of development.

IV. CONCLUSION:

In the current paper, we further present the method of de-correlation of the speckle pattern in the elevation direction to determine the scan plane relative positions and their motions. The experimental results based on a tissue-mimicking phantom seems good for the current technique. However, the current method for the de-correlation of the speckle can only be applied to a clinical set when tissue can be modeled as a gelatin matrix containing many small randomly distributed point-like scatterers. Nevertheless, the current method should serve as a baseline for the motion detection based on the de-correlation of speckles.

ACKNOWLEDGMENTS

REFERENCE

1. J.F. Chen, J.B. Fowlkes, and P.L. Carson, "Determination of scan plane motion using speckle de-correlation. Part I, theoretical consideration and initial testing," J. Acoust. Soc. Am., (submitted).

2. R.F. Wagner, S.W. Smith, J.M. Sandrik, and H. Lopez, "Statistics of speckle in ultrasound B-scans," IEEE Trans. Sonics Ultrason., vol. SU-30, pp 156-163 (1983).

3. L. Nock, G.E. Trahey, "Phase aberration correction in medical ultrasound using speckle brightness as a quality factor," J. Acoust. Soc. Am., 85, pp 1819-1833 (1989).

4. P.B. Bevington, Data Reduction and Error Analysis for Physical Science (McGraw-Hill, New York, 1969).

5. M.F. Insana and T.J. Hall, "Visual detection efficiency in ultrasonic imaging: A framework for objective assessment of image quality," J. Acoust. Soc. Am., 95, pp 2081-2090 (1994).

6. J.F. Chen, J.A. Zagzebski and E.L. Madsen, "Statistical uncertainty in estimates of an effective scatterer number density for ultrasound," J. Acoust. Soc. Am., 96, pp 2556-2563 (1994).

7. M.F. Insana and T.J. Hall, "Visual detection efficiency in ultrasonic imaging: A framework for objective assessment of image quality," J. Acoust. Soc. Am., 95, pp 2556-2563 (1994).

8. R.S. Adler, J.M. Rubin, J.B. Fowlkes, P.L. Carson, and J.E. Pallister, "Ultrasonic estimation of tissue perfusion: a stochastic approach," Ultrason. in Med. & Biol., (accepted).

Figure 1: The normalized auto-correlation function of echo signal intensity based on the region of interest in the focal region or in the far-field region. The solid line is the result based on Equation (11), while the dash line is the result of Gaussian fitting curve.

Figure 2: When the scan-plane is automatically scanned through a tissue mimicking phantom in the elevation direction, the normalized correlation function of echo intensities as a function of different number of steps.

Figure 3: When the scan-plane is manually scanned through a tissue mimicking phantom in the elevation direction, the normalized correlation function of echo intensities as a function of different number of steps.

Figure 4: Left to right (1) The reconstruction of a longitudinal view of cone object in the contrast detail phantom from a 3.5 MHz array transducer using assuming equal step size; (2) The reconstruction of the same view using manually actual step size estimated by the correlation of speckle; (3) The subtract image between these two views. The left graph shows the step size changed with the step number, and the right graph shows the integrated step size changed with the step number.
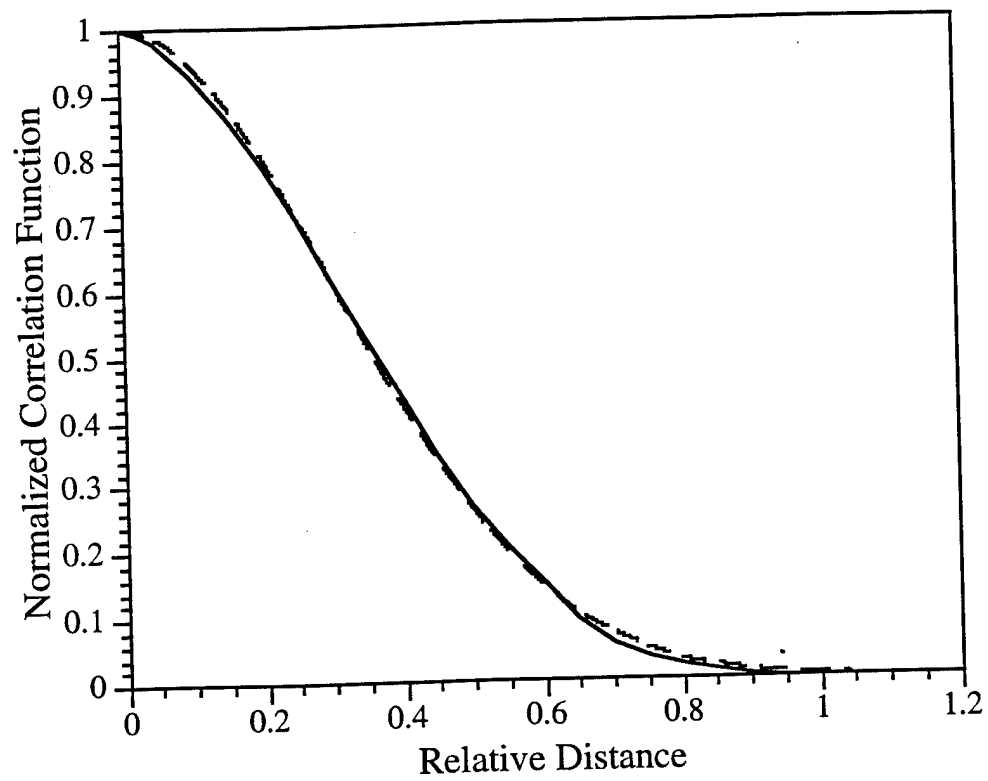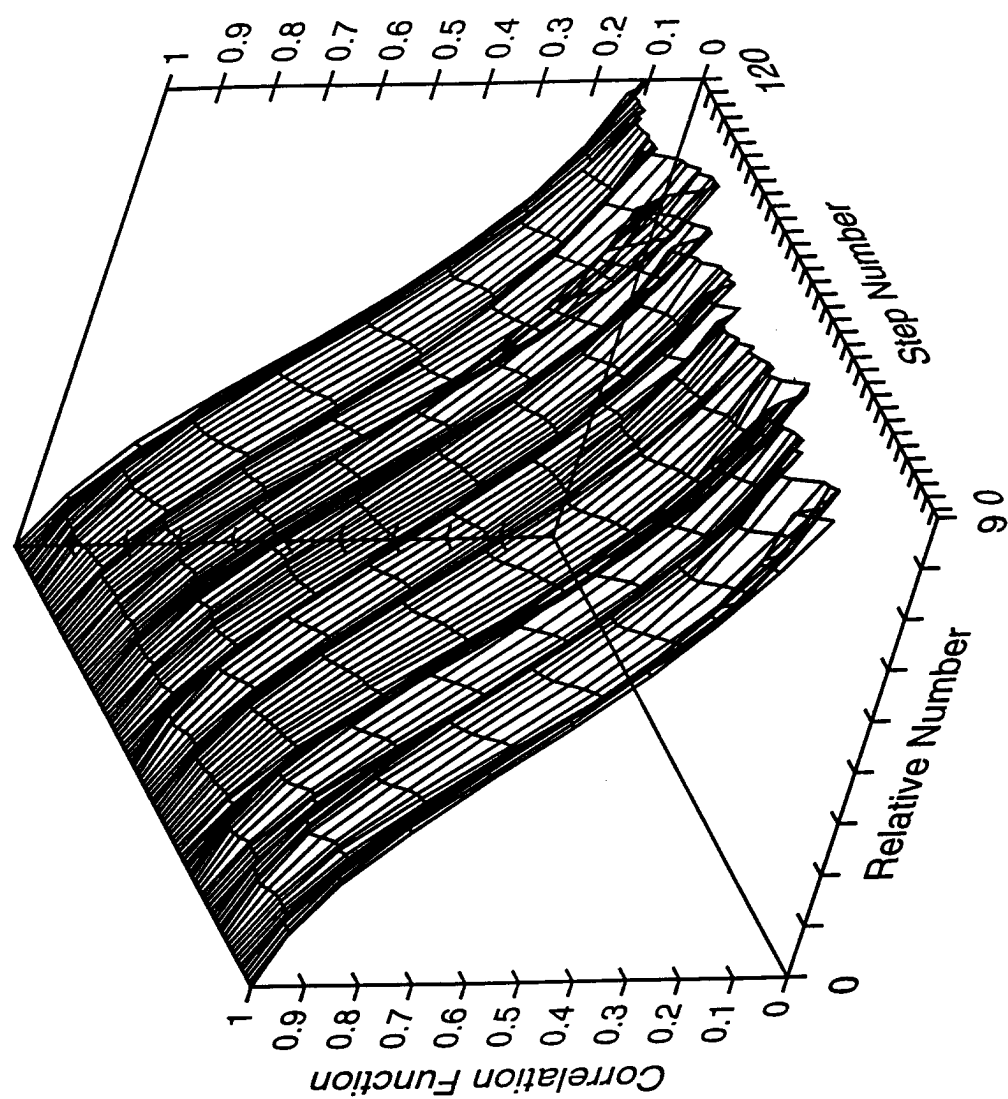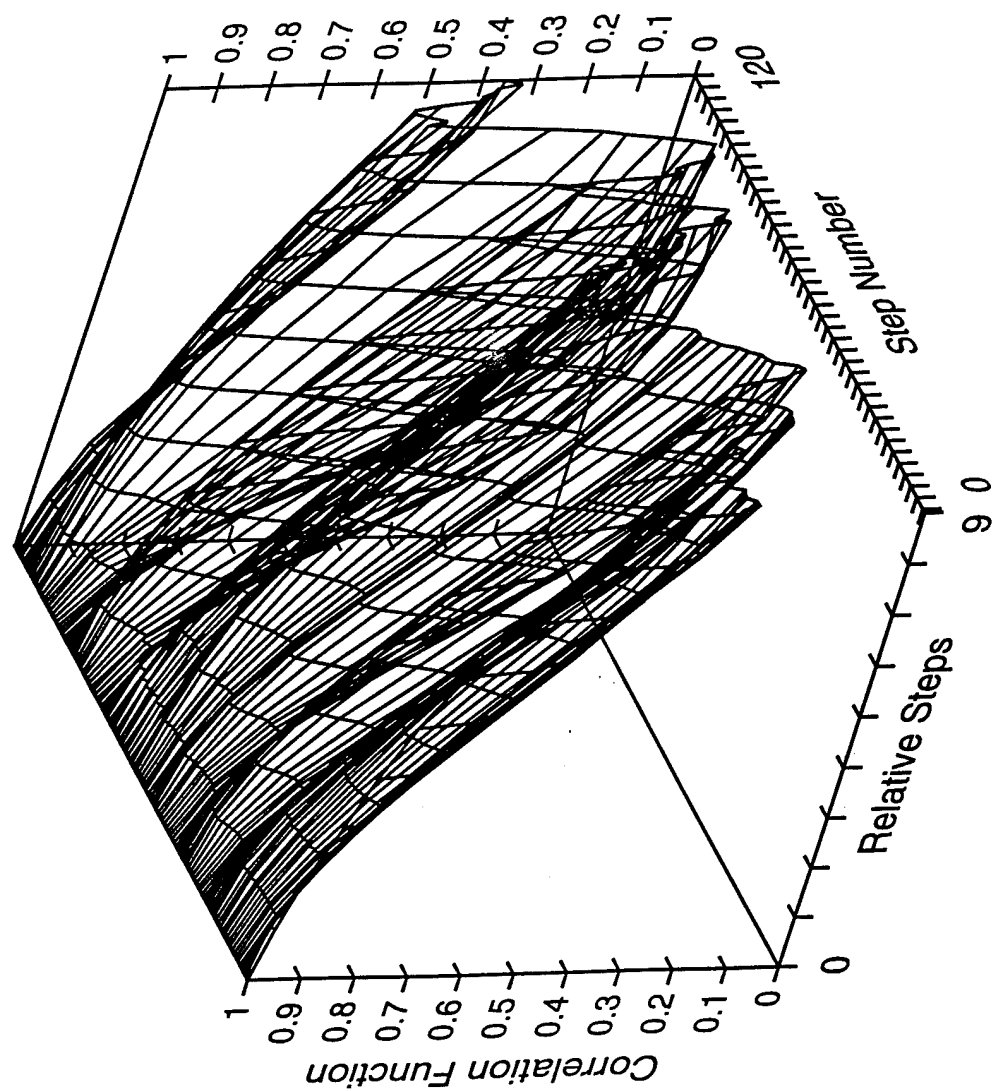
Figure 1

Figure 2

Figure 3